Precambrian Research 275 (2016) 429–449

Contents lists available at ScienceDirect

Precambrian Research

journal homepage: www.elsevier.com/locate/precamres

Microstructure-specific carbon isotopic signatures of organic matter from ~3.5 Ga cherts of the Pilbara Craton support a biologic origin

Navot Morag[a,*], Kenneth H. Williford[a,b], Kouki Kitajima[a], Pascal Philippot[c], Martin J. Van Kranendonk[d], Kevin Lepot[a,e], Christophe Thomazo[c,f], John W. Valley[a]

[a] NASA Astrobiology Institute, WiscSIMS, Department of Geoscience, University of Wisconsin, 1215 W. Dayton St., Madison, WI 53706, USA
[b] Jet Propulsion Laboratory, California Institute of Technology, Pasadena, CA 91109, USA
[c] Institut de Physique du Globe de Paris, CNRS and Université Denis Diderot, 4 place Jussieu, 75005 Paris Cedex, France
[d] School of Biological, Earth and Environmental Sciences, and Australian Centre for Astrobiology, University of New South Wales Australia, Kensington, NSW 2052, Australia
[e] Laboratoire Géosystèmes, Université Lille 1, CNRS UMR8217, 59655 Villeneuve d'Ascq, France
[f] UMR CNRS/uB5561 Biogéosciences UFR Sciences Vie Terre Environnement, Université de Bourgogne, 6 Bd. Gabriel, 21000 Dijon, France

ARTICLE INFO

Article history:
Received 7 July 2015
Received in revised form 7 December 2015
Accepted 6 January 2016
Available online 22 January 2016

Keywords:
Dresser Formation
Organic matter
Carbon isotope ratio
SIMS
Microfossils
Pilbara craton

ABSTRACT

The ~3.5 Ga Dresser Formation from the North Pole Dome of the Pilbara Craton (Western Australia) contains some of the oldest evidence for life on Earth. Here, we present a detailed study of microstructure-specific carbon isotopic composition of organic matter (OM) preserved in Dresser Formation bedded cherts and hydrothermal chert vein using in situ Secondary-Ion Mass Spectrometry (SIMS). The OM in these rocks occurs mainly as clots that, together with minor fine OM layers and laminae, are considered primary textures formed prior to host rock lithification. Other than rare OM-rich stylolites, no evidence was found for later OM migration beyond the micrometer scale. Average $\delta^{13}C$(OM) values in specific microstructural types range between −33.6‰ and −25.7‰. No correlation is seen between measured $\delta^{13}C$ values and H/C ratios in the studied OM microstructures. This lack of correlation and the low metamorphic grade of the rocks studied argue against significant modification of OM isotopic composition by later metamorphic alteration. It is thus concluded that the range of $\delta^{13}C$ values found in the samples represents primary OM isotopic variability. Within some individual samples variable $\delta^{13}C$(OM) values are correlated with specific microstructural types. This observation is not consistent with solely abiotic OM formation via Fisher-Tropsch type reactions. When compared with associated $\delta^{13}C$(ankerite) values, average $\delta^{13}C$(OM) values indicate C isotopic fractionation [$\Delta^{13}C$(Ank–OM)] of 25–33‰, which translates to dissolved CO_2–OM isotopic fractionation [$\Delta^{13}C(CO_2–OM)$] of 20–30‰. This range of $\Delta^{13}C(CO_2–OM)$ is consistent with enzymatic C fixation via the Calvin cycle utilized by photoautotrophs and the reductive acetyl-CoA pathway utilized by chemolithoautotrophs. Photosynthetic OM formation is supported by the relatively shallow water depth inferred for the Dresser environment and the restricted occurrence of stromatolites to shallow water deposits in this unit, whereas chemolithosynthesis is supported by the abundance of OM in sub-seafloor hydrothermal chert veins. The range of $\delta^{13}C$(OM) values observed in the samples may therefore represent the remains of different organisms utilizing different C-fixation pathways. Other biologic effects, such as the growth rate and density of microbial communities, and further heterotrophic overprinting of the autotrophic biomass may have also contributed to the observed range of $\delta^{13}C$(OM) values.

1. Introduction

The North Pole Dome of the Pilbara Craton in Western Australia is well-known as the site of Earth's oldest putative stromatolites and microfossils occurring in ca. 3.5 Ga bedded chert-barite deposits of the Dresser Formation of the Warrawoona Group (Awramik et al., 1983; Walter et al., 1980). Although the biogenicity of these early structures have been debated (Buick, 1984, 1990; Buick et al., 1981), there is ample evidence in support of the existence of an early biosphere in the Dresser Formation, including the link between alleged biogenic structures and organic matter (OM) distribution (Glikson et al., 2008; Harris et al., 2009; Ueno et al.,

* Corresponding author.
E-mail address: morag@wisc.edu (N. Morag).

http://dx.doi.org/10.1016/j.precamres.2016.01.014
0301-9268/

2004; Van Kranendonk, 2011; Van Kranendonk et al., 2008), the isotopic signature of sulfur in microscopic sulfides, which suggest sulfur-based metabolism (Philippot et al., 2007; Shen et al., 2001; Ueno et al., 2008), and the carbon isotopic composition of methane in fluid inclusions, which is similar to that of microbially produced methane (Ueno et al., 2006). One of the prominent features of the Dresser Formation, and the Warrawoona Group in general, is the common occurrence of black-gray OM-bearing cherts. These cherts occur both as layered cherts interbedded within the stratigraphic succession and as hydrothermal veins–sometimes referred to as 'silica dikes', which cut across the local stratigraphy before truncating abruptly at specific overlying stratigraphic horizons, interpreted as the fossil seafloor, where they usually interfinger with the bedded cherts (e.g. Lindsay et al., 2005; Nijman et al., 1999; Van Kranendonk, 2006; Van Kranendonk et al., 2008). The source of OM contained in these cherts is enigmatic and may have significant implications regarding the emergence of early Archean biosphere – is it biogenic, and thus indicative of early life (e.g. Ueno et al., 2004), or abiogenic, and perhaps serving as a source of prebiotic compounds that led to the appearance of life (e.g. Lindsay et al., 2005)? Previous studies have shown that OM in the chert veins and bedded cherts is low in $\delta^{13}C$ in a manner comparable to that of organic carbon fixed by autotrophic organisms (Hayes et al., 1983; Pinti et al., 2009a; Ueno et al., 2001, 2004). However, some studies have argued that similar low values of $\delta^{13}C$ may form during the production of organic compounds by abiotic processes similar to the industrial Fischer-Tropsch synthesis and thus concluded that the isotopic composition of the OM by itself does not provide conclusive evidence for a biogenic origin (Brasier et al., 2002; Lindsay et al., 2005; McCollom and Seewald, 2006).

OM in the Dresser Formation bedded cherts and associated hydrothermal chert veins shows variable bulk (mm- to cm-scale) $\delta^{13}C$ values, between −38‰ and −29‰ VPDB, interpreted as resulting from varying degrees of post-depositional metasomatic alteration (oxidation) (Ueno et al., 2004) or hydrothermal/metamorphic alteration (Pinti et al., 2009a). A detailed study of OM preserved in these rocks using organic petrology and scanning and transmission electron microscopy has revealed the occurrence of several morphologically-distinct OM populations, indicating potentially different sources and/or subsequent degradation/maturation processes (Glikson et al., 2008). These findings demonstrate the inherent difficulty in interpretation of bulk OM data and the need to consider the petrographic context of the carbonaceous microstructures. In situ (micron-scale) C-isotope analysis using Secondary-Ion Mass Spectrometry (SIMS) may provide further important data about the origin of OM since it is capable of distinguishing between different generations of OM in the cherts, whose unique isotopic composition may be averaged or completely obscured by conventional bulk analysis. Hitherto, in situ C isotope analyses of OM in the Warrawoona Group have targeted only rare carbonaceous filaments, which may represent fossil bacteria, and associated carbonaceous clots in two chert vein samples (Ueno et al., 2001). Furthermore, these analyses were standardized against a sample of crystalline graphite, which differs from the kerogenous OM found in the cherts, creating differences in the instrumental mass bias and thus potential errors in analysis (House et al., 2000; McKeegan et al., 1985; Williford et al., 2013).

This study presents a new, comprehensive data set of kerogen-standardized in situ SIMS $\delta^{13}C$ analyses of specific OM microstructures and associated carbonates for unweathered samples recovered from the PDP2b and 2c drillcores (Van Kranendonk et al., 2008) of the lowermost chert-barite unit of the ~3.5 Ga Dresser Formation, which represent Earth's oldest proposed fossiliferous sedimentary rocks (Ueno et al., 2001; Van Kranendonk, 2011; Van Kranendonk et al., 2008; Walter et al., 1980). Our data provide new insights as to the origin, migration and alteration of OM preserved in these rocks.

2. Geologic setting and sampling

The Dresser Formation is a package of interbedded chert-barite units and pillow basalts within the lower part of the Warrawoona Group of the Pilbara Supergroup (Van Kranendonk et al., 2007). Exposed only in the North Pole Dome, the Dresser Formation is preserved as a ring of hills, about 14 km in diameter, centered around the younger North Pole Monzogranite that was emplaced into the core of the dome at ~3.46 Ga (Van Kranendonk et al., 2008) (Fig. 1). The potentially fossiliferous, bedded chert-barite unit at the base of the Dresser Formation varies between 4 and 60 m in thickness (Van Kranendonk et al., 2008). It is composed of predominantly bedded chert, thick units of coarsely crystalline barite, conglomerate, sandstone and carbonates (Buick and Dunlop, 1990; Hickman, 1983; Nijman et al., 1999; Van Kranendonk, 2006; Van Kranendonk et al., 2008). The bedded chert-barite unit is underlain by pervasively hydrothermally altered komatiitic basalt transected by numerous veins of black-gray chert, varying up to ~20 m wide and up to 2 km long, which are thought to represent conduits of hydrothermal circulation (Isozaki et al., 1997; Nijman et al., 1999; Ueno et al., 2004; Van Kranendonk, 2006).

Two Pb–Pb model ages of ~3.49 Ga on galena in barite were previously cited as the age of the formation (Thorpe et al., 1992a), but recent U–Pb zircon dating of a felsic volcaniclastic sandstone from the top of the lowermost chert unit of the formation has yielded a maximum depositional age of 3.481 ± 0.002 Ga, which is interpreted to represent the age of deposition of this unit (Van Kranendonk et al., 2008). ^{147}Sm–^{143}Nd data from hydrothermally-altered metabasalts and basaltic metakomatiites, stratiform barite and black chert veins (from the studied PDP drill cores) yielded an isochron age of 3.49 ± 0.10 Ga, confirming the U-Pb and Pb-Pb ages (Tessalina et al., 2010). Overlying volcanics and related intrusions in the North Pole Dome have been dated at between 3.46 and 3.44 Ga (Amelin et al., 2000; Thorpe et al., 1992b).

Regional studies of metamorphic assemblages in the North Pole metabasalts show a locally variable pattern of metamorphic overprint. Peak metamorphic temperatures range from ~150 °C up to ~350 °C and show a general repeated pattern of increasing temperature with stratigraphic depth within the sequences of basalt-chert packages that comprise the North Pole Dome section (Kitajima et al., 2001; Terabayashi et al., 2003). However, in places the metamorphic conditions also vary considerably horizontally, within the sedimentary beds and basalt flows in relation with the occurrence of hydrothermal veins. This style of metamorphism was interpreted to result from repeated episodes of hydrothermal circulation within volcanic packages separated by silicified sediments that acted as aquacludes to hydrothermal fluid circulation (Van Kranendonk, 2006).

The Raman spectra acquired for the OM in different OM-bearing chert units of the North Pole Dome are generally similar to those of kerogen from lower greenschist facies metasedimentary rocks (Marshall et al., 2012; Ueno et al., 2004; Wacey et al., 2011b), although lower-temperature hydrothermal conditions of ~100–300 °C have been reported from the study of mineral assemblages (kaolinite-quartz: Van Kranendonk, 2006; Van Kranendonk and Pirajno, 2004) and fluid inclusions in cherts and adjacent metabasalts (Foriel et al., 2004; Harris et al., 2009).

The samples studied here come from the drill cores of the Pilbara Drilling Project site #2 (PDP2) collected in 2004 as part of a scientific collaboration between the Institut de Physique du Globe de Paris and the Geological Survey of Western Australia (for details see Van Kranendonk et al., 2008). Six samples were selected from

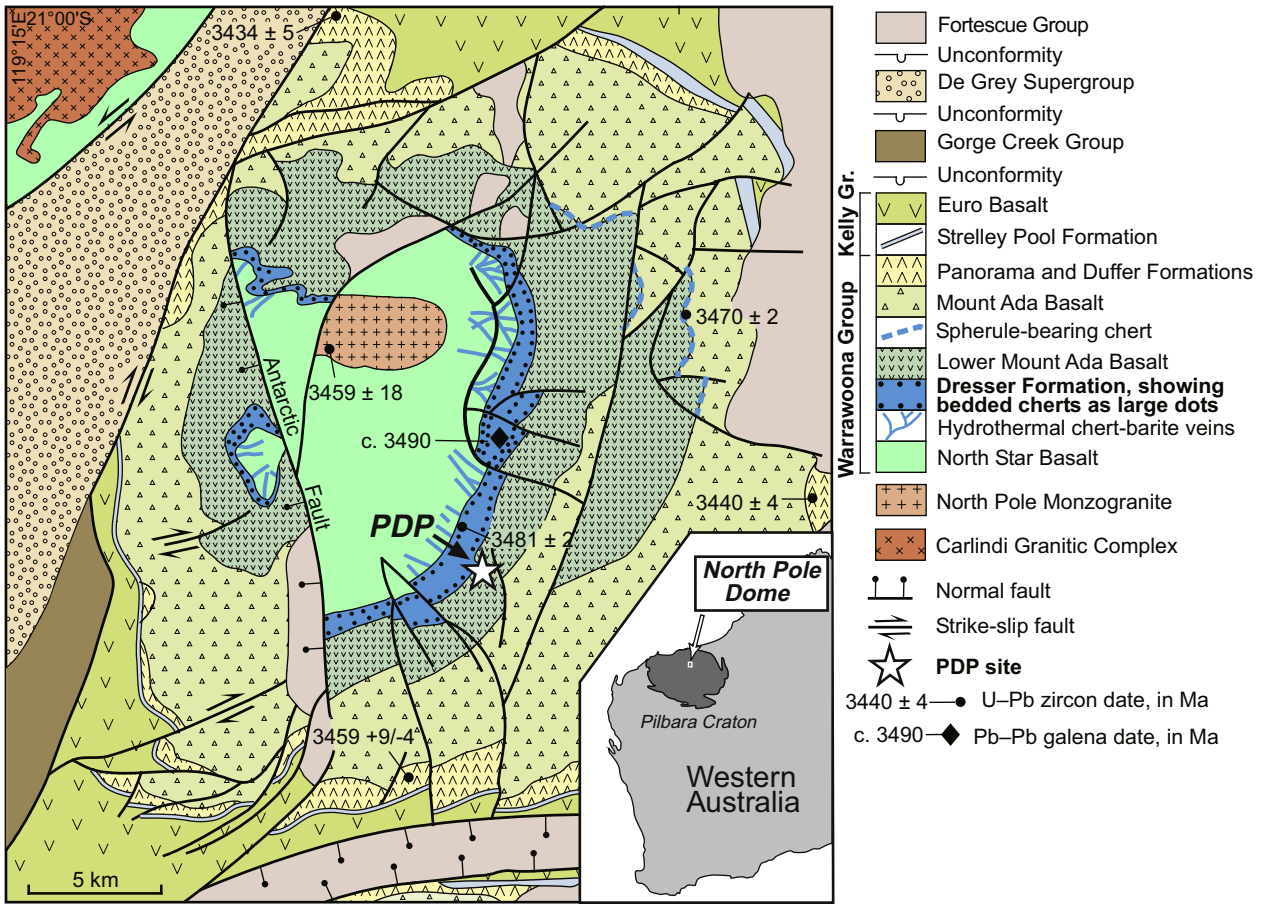

Fig. 1. Geological map of the North Pole Dome in the Pilbara craton, Western Australia showing the location of the PDP2 drill site. Modified after Van Kranendonk (2010).

the bedded chert-carbonate member 6 of the PDP2b and PDP2c drill cores and one sample was selected from a dark-gray chert vein transecting the altered komatiitic basalt below the bedded chert-barite unit in drill core PDP2c (Fig. 2).

3. Methods

3.1. Microscopy

Approximately 100-μm thick, doubly polished thin sections were prepared from each sample. After preliminary optical inspection under a microscope using transmitted light the sections were detached from the carrier glass and fragments (1–3 mm wide) of selected areas were broken off, embedded in circular 25.4 mm diameter epoxy mounts, and ground and repolished to expose OM features of interest. The OM microstructures to be analyzed in these mounts were selected, studied and imaged using a Nikon Eclipse E600 microscope under transmitted light and reflected light. Scanning electron microscope (SEM) images were acquired in backscattered electron (BSE) mode on thinly gold-coated (~5 nm) samples using a Hitachi S3400 SEM operated at 10–15 kV and a working distance of 10 mm. BSE images were recorded before and after SIMS analyses.

3.2. Bulk carbon isotope analysis

Bulk rock samples were powdered to <60 μm using a zirconium oxide crusher. Powders were homogenized, sieved and aliquots were used for organic carbon isotope analyses.

Total organic carbon content (TOC) and organic carbon isotope composition [$\delta^{13}C(OM)$] were measured on carbonate-free residues. Sample powders were rinsed by dichloromethane–ethanol (9:1) to remove any modern organic contaminant and reacted with HCl (6 N) at room temperature overnight followed by 4 h at 80 °C to remove carbonates. Residues were rinsed with deionized distilled water to a neutral pH, centrifuged (3500 rpm for 5 min), and dried at 60 °C overnight. Aliquots of dried decarbonated samples (100–200 mg) were then sealed in evacuated quartz tubes together with CuO wires and combusted at 950 °C for 6 h. The produced CO_2 was purified in a vacuum line and yield was measured manometrically, allowing TOC determination with a reproducibility better than ±0.03 wt.% (1σ). Carbon isotope composition of the purified CO_2 gas was measured on a delta+XP mass spectrometer at the Institut de Physqiue du Globe de Paris with a precision better than ±0.4‰ (1σ) based on duplicate analyses of samples and standards. Results are reported in the delta notation in ‰, relative to V-PDB (Sup. data Table S1).

3.3. SIMS carbon isotope analysis

SIMS analyses of carbon isotope ratios were performed on selected OM microstructures identified in the thin sections studied. Prior to analysis, a ~200 nm gold coat was applied to facilitate charge compensation during SIMS analysis, and all samples were degassed at 10^{-9} Torr in the SIMS air-lock sample chamber for >12 h. Analyses were carried out using a CAMECA IMS 1280 at the WiscSIMS laboratory, UW-Madison, following the procedure described in Williford et al. (2013) and Lepot et al. (2013). A

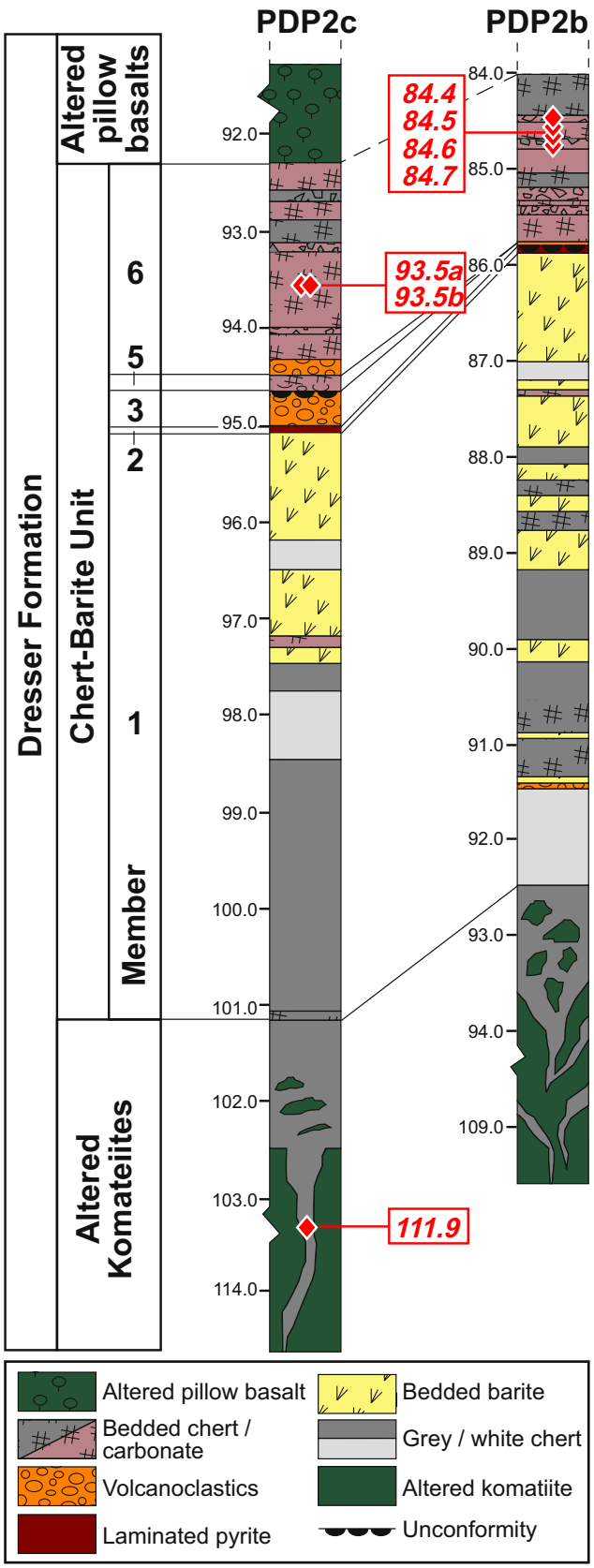

Fig. 2. Stratigraphic logs of drillcores PDP2b and PDP2c showing the location of the samples studied (red diamonds). Numbers to the left of each log indicate depth in meters down the drill hole. Sample numbers in red are keyed to depth. Modified after Van Kranendonk et al. (2008).

$^{133}Cs^+$ primary ion beam with 20 kV total impact voltage and ~2.5 nA intensity was focused into an ellipse of ~15 μm maximum dimension at the sample surface. Secondary ions were counted simultaneously using the following detector setup: $^{12}C^-$ [(Faraday cup (FC) at the L′2 position with a 10^{11} Ω resistor, mass resolution $M/\Delta M = 2200$], $^{13}C^-$ [axial electron multiplier (EM), $M/\Delta M = 4000$], and $^{13}CH^-$ (EM at the H2 position, $M/\Delta M = 2200$). DTFA (first deflector of transfer optics for centering secondary ions in the field aperture) X and Y parameters were adjusted by rastering the primary beam over a 25 × 25 μm area near each target area and applying the dynamic transfer plate voltage synchronized with primary beam rastering to obtain stable secondary ion intensity. Each analysis consisted of 70 s of presputtering and a total counting time of 160 s (80 measurement cycles of 2 s each). Values of $\delta^{13}C_{Raw}$ (in ‰) represent the $^{13}C/^{12}C$ isotopic ratio measured by SIMS reported against the value for VPDB before correction for instrumental bias.

Standardization of measurements is critical for establishing the accuracy of SIMS analyses, a problem arising chiefly from systematic bias that occurs during analysis. This instrumental bias can be measured and corrected by bracketing sample analyses with analyses of a working standard of known isotopic composition and with a chemical composition and matrix similar to that of the sample (e.g. Eiler et al., 1997; Kita et al., 2009). In certain crystalline materials, the crystal structure and orientation can also affect bias (Huberty et al., 2010; Kozdon et al., 2010). In the case of SIMS carbon isotope analysis, the bias for graphite is different than that for amorphous carbonaceous matter such as kerogen or coal (by as much as 10‰; House et al., 2000). Moreover, an orientation effect of several per mil has been observed in C isotopic measurements of individual graphite crystals in the WiscSIMS laboratory (T. Ushikubo, unpublished data). A strong systematic correlation between SIMS instrumental bias and H/C ratio was also reported within two suites of natural organic carbon samples analyzed in two different laboratories (Sangély et al., 2005; Williford et al., in press). For this study we used an epoxy-embedded chip of the carbonaceous chert sample PPRG-215 (Walter et al., 1983), the same sample used as a working standard by House et al. (2000), Williford et al. (2013) and Lepot et al. (2013) to measure carbon isotope compositions of individual Precambrian microfossils. Each set of ~12 sample analyses was bracketed by eight analyses of the PPRG-215 standard (Sup. data Table S2). Instrumental bias (α_{SIMS}) was calculated by comparing the average $\delta^{13}C_{Raw}$ for the eight bracketing analyses of PPRG-215 to the published value of −31.5‰ (VPDB; Hayes et al., 1983) using the following equation (see also Kita et al., 2009):

$$\alpha_{SIMS} = \frac{1 + (\delta^{13}C_{Raw}/1000)}{1 + (-31.5/1000)} \quad (1)$$

This factor, α_{SIMS}, was then used to correct raw values from sample analyses using the following equation:

$$\delta^{13}C_{VPDB} = \left[(1 + \delta^{13}C_{Raw}/1000)/\alpha_{SIMS} - 1\right] \times 1000 \quad (2)$$

The analytical error for each OM sample analysis was calculated as the quadratic addition of the internal precision, calculated as two standard errors (2SE) on the sample's 80 measurement cycles, and the external precision, calculated as the two standard deviations (2SD) on the eight bracketing standard analyses.

The ^{12}C count rates for 70 analyses of the PPRG-215 standard ranged between 2.4×10^6 and 18.5×10^6 counts per second (cps) (Sup. data Table S2). Analyses with low carbon concentrations (^{12}C count rates $<1 \times 10^6$ cps ≈ 10% of the average count rates for bracketing standards) were rejected, as internal precision decreases significantly relative to external precision (reproducibility of bracketing standards) at such low ^{12}C count rates, largely due to Poisson counting statistics (Williford et al., 2013). No correlation was found

between ^{12}C cps and $\delta^{13}C_{Raw}$ values in the studied OM samples (Sup. data Fig. S1).

In some of the studied samples, coexisting carbonates [ankerites; 15–28 mol.% Fe (percentage of Fe from total cations – Ca, Sr, Mg, Fe, Mn), Fe/(Fe + Mg) = 0.33–0.61] were analyzed during the organic carbon analytical session using similar instrumental settings. The cation composition within the dolomite-ankerite solid solutions introduce systematic differences in bias of the measured C isotope ratios, sometimes referred to as the matrix effect (Valley and Kita, 2009). In order to correct for this matrix effect, we applied a correction scheme based on the correlation of matrix-induced bias and Fe content in carbonates within a set of three carbonate standards. Carbonate analyses were bracketed by eight analyses of the UWC-3 calcite standard. Two secondary standards of dolomite, UW6220 [0.1 mol.% Fe, Fe/(Fe + Mg) = 0.002], and ankerite, UWAnk-1 [24.6 mol.% Fe, Fe/(Fe + Mg) = 0.52], were analyzed at the end of the session. A calibration curve for Fe content was fitted by Hill equation using the UW6220 and UWAnk-1 standards following the method described by Śliwiński et al. (in press). The matrix dependent bias was calculated for each carbonate analysis pit using this calibration curve normalized to the average α_{SIMS} attained for the eight bracketing analyses of UWC-3, and the crystal's specific cation composition measured adjacent to each SIMS analysis pit by electron microprobe (EMP; Sup. data Table S3).

4. Results

4.1. OM microstructures

Several different types of OM microstructures were identified and classified within the studied samples. Some of the samples contained only one type of OM microstructure, whereas others included a variety of OM microstructures. The following is a description of individual samples and the OM microstructures found within them.

- ***Sample 84.4*** (PDP2b) is a bedded chert, perhaps representing a silicified carbonate unit, comprising alternating light and dark-colored layers that differ in their OM content (Fig. 3a). Up to ~5 vol.% carbonate is present as isolated euhedral to subhedral crystals of dolomite-ankerite. OM in this sample occurs as: (1) discrete clots of amorphous shape and relatively small size, typically <50 μm, comprised of nano to microscale granular OM distributed mainly along the grain boundaries of micro-quartz crystals, 1–10 μm in diameter. The clots occur both in the darker, OM-rich beds, together with dispersed layered OM (see below) and in the lighter-colored beds, which are otherwise depleted in OM (Fig. 3a). Some of the clots in the OM-depleted beds display irregular, yet more distinct shapes with relatively concentrated thread-like OM domains. Based on these observations the clots in this sample were divided into OM-rich beds 'Type-1' clots and OM-poor beds 'Type-2' clots (Fig. 4a and b, respectively). (2) Dispersed layered OM that comprises the darker OM-rich layers. Sub-micrometer scale OM in these layers is sparsely distributed mostly along micro-quartz grain boundaries (Fig. 4c). (3) OM concentrated along serrated fronts that run more or less parallel to the bedding plains and resemble stylolitic fronts (Fig. 3a). These stylolitic fronts usually separate light OM-depleted layers from darker OM-rich layers and probably represent migration and concentration of OM during primary carbonate dissolution. The OM along these stylolites occurs as lumps of concentrated OM of variable size (Fig. 4d). Along some of the well-developed fronts OM lumps may reach relatively large size up to ~30 μm (Sup. data Fig. S2). The most massive lumps were not targeted in this study as they were too concentrated to be analyzed under the instrument analytical settings (i.e. the use of EM detectors for measurements of ^{13}C and ^{13}CH intensity), but they appear to be texturally similar to smaller (<5 μm) lumps that were analyzed. Stylolites are often accompanied by chlorite (Fig. 4d). (4) OM filling rare small micron-scale cracks/fissures (Sup. data Fig. S3; a10_1b). (5) OM enclosed in the core of euhedral carbonate rhombs (Sup. data Fig. S2). This form of OM was not analyzed in this study due to the difficulty in distinguishing the C signal of OM from that of the host carbonate.
- ***Sample 84.5*** (PDP2b) is a bedded chert/silicified carbonate comprised of two main beds, a dark-colored OM-rich bed overlaying a light-colored bed devoid of OM. The two beds are separated by a dark well-developed stylolite front containing massive chlorite (Fig. 3b). Rare (<5 vol.%) ankerite [~25 mol.% Fe, Fe/(Fe + Mg) = 0.53] is present as isolated euhedral crystals. OM is present as: (1) Widespread discrete clots of amorphous shape and variable size, typically 50–200 μm, comprising a dense network of nano- to micro-granular OM distributed mainly along micro-quartz grain boundaries (Fig. 4e). The clots occur only in the darker OM-rich bed. (2) OM concentrated along the stylolitic front (Fig. 3b; Sup. data Fig. S2). OM in stylolites was not analyzed in this sample as it resided in massive chlorite matrix, whose effect on the instrument bias cannot be corrected, and was too concentrated to be analyzed under the instrument analytical settings.
- ***Sample 84.6*** (PDP2b) is a bedded chert/silicified carbonate (Fig. 3c) containing <5 vol.% carbonates, which occur as euhedral crystals of dolomite-ankerite, containing small (<10 μm) inclusions of siderite. OM in this sample occurs as discrete clots of relatively concentrated OM of amorphous shape and variable size, typically 50–100 μm in length, comprised of nano- to micro-granular OM (Fig. 4g). Some nano-granular OM is distributed along micro-quartz grain boundaries. A stylolitic front within this sample is marked by the presence of chlorite, however, no OM concentration is seen along this front and it does not separate OM-rich and OM-depleted regions as in other samples (Fig. 3c; Sup. data Fig. S3).
- ***Sample 84.7***(PDP2b) is a dark-colored, very OM-rich, bedded chert/silicified carbonate (Fig. 3d). The rock contains 5–10 vol.% carbonate, which occurs as large, mostly subhedral to anhedral crystals of ankerite [15–28 mol.% Fe, Fe/(Fe + Mg) = 0.33–0.61]. Some of the carbonates are partly altered to Fe-oxides and chlorite. Rare sulfides (pyrite, chalcopyrite) are also present as isolated euhedral crystals. OM microstructures in this sample include: (1) Clots of relatively concentrated OM of amorphous shape and variable size, up to ~500 μm long, comprised of nano- to micro-granular OM. The clots appear to be faintly laminated, with their elongated axis mostly parallel to the main bedding. (2) Laminated OM, which appears as fine laminae, typically thinner than 50 μm, of amorphous OM surrounding grains of silicified clastic (clay/silt-sized) material (Fig. 3d). The clots and laminae occur at separate beds, although the transition between those beds is not well defined. The laminae microstructures may resemble the network-forming laminae described in the Dresser Formation by Noffke et al. (2013), who interpreted them to be typical of microbial mat growth. The OM in the clots and laminae is rather similar, comprised of nano- to micro-granular texture (Fig. 4h).
- ***Sample 93.5a*** (PDP2c) is a partly silicified bedded carbonate comprised of a bed/vein of coarse-grained dolomite-ankerite partly replaced by chlorite with rare quartz and TiO_2, mostly devoid of OM, and a bed of intensely silicified, finer grained carbonates (Fig. 3e) comprising about 50% microcrystalline quartz and ~50% subhedral dolomite-ankerite with small (<10 μm) inclusions of siderite. OM occurs in the latter as rare, amorphous clots of OM of relatively small size, <50 μm, comprised of nano- to

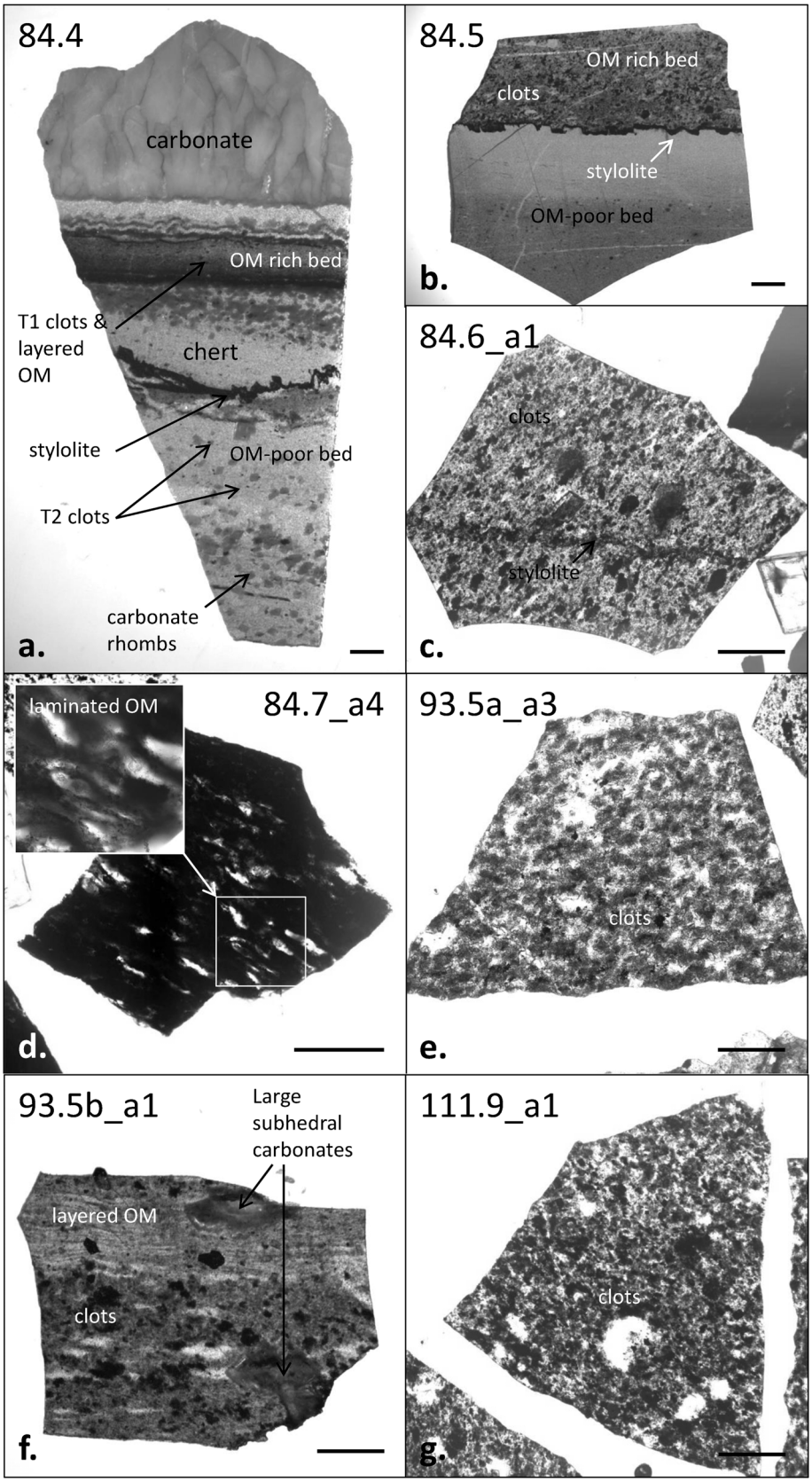

Fig. 3. Low-magnification transmitted-light images of OM microstructures in the samples studied. Scale bars are 1 mm.

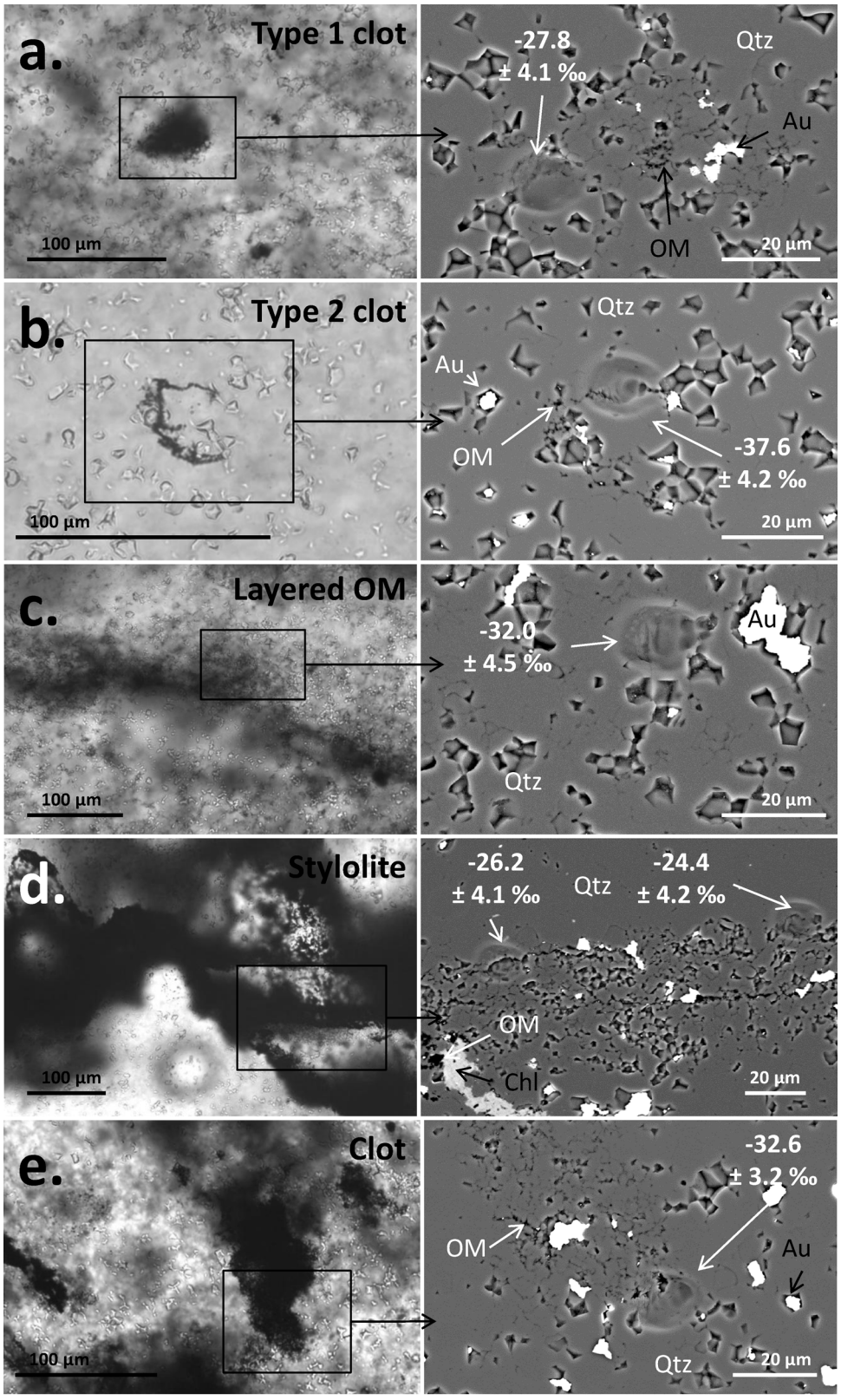

Fig. 4. Matching transmitted light (TL; left) and Back-Scattered Electron (BSE; right) images of selected SIMS pits. a, b, c and d – Type 1 clot, Type 2 clot, layered OM and stylolite, respectively, in sample 84.4; e and f – clot and carbonate, respectively, in sample 84.5; g – clot in sample 84.6; h – laminated OM in sample 84.7; i – clot in sample 93.5a; j – clot and stylolite in sample 93.5b; k and l – clot and carbonate, respectively, in sample 111.9. The light hue ovals in the BSE images are the SIMS analysis pits. The $\delta^{13}C(OM)_{VPDB}$ values obtained for the pits are shown with the BSE images. *Abbreviations*: Au, remnants of gold coating (not part of the original assemblage); Carb, carbonate (dolomite-ankerite), Chl, chlorite; OM, organic matter; Py, pyrite; Qtz, quartz. The complete dataset of TL and BSE images for all studied SIMS pits is given in Sup. data Fig. S3.

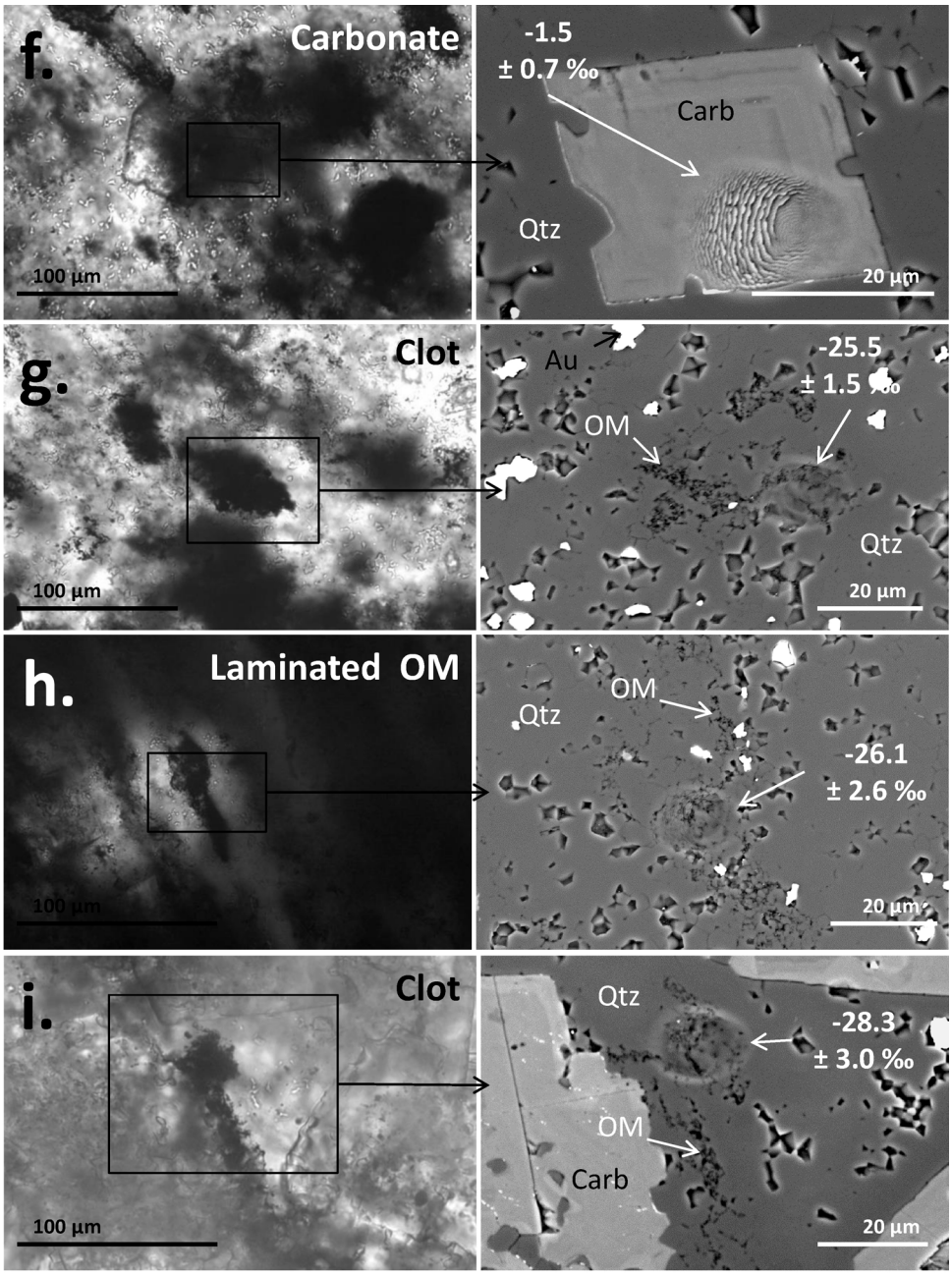

Fig. 4. (*Continued*)

micro-scale granular OM (Fig. 4i). The clots occur in both carbonate and quartz matrix, however, in this study we have analyzed $\delta^{13}C$ only in clots that reside in the quartz matrix because of the difficulty in distinguishing the C signal of OM and that of the host carbonate.

- ***Sample 93.5b*** (PDP2c) is a bedded chert/silicified carbonate containing large patches of subhedral carbonates (dolomite-ankerite; ~20–30 vol.%) and smaller rare (~5 vol.%) ankerite rhombs [24–27 mol.% Fe, Fe/(Fe + Mg) = 0.53–0.56] scattered in the quartz matrix (Fig. 3f). Scattered chlorite (~5 vol.%) is also found in the chert matrix. OM in this sample is present as: (1) Discrete clots of relatively concentrated OM of amorphous shape and variable size, typically 50–100 µm, comprised of nano- to micro-granular OM (Fig. 4j). (2) Faint layers of dispersed OM comprised of nanometer scale OM distributed along micro-quartz grain boundaries. The OM clots and layered OM occur mostly within separate beds (Fig. 3f). (3) OM concentrated along rare stylolites, comprised of small, few micron-scale chunks of OM mostly embedded in chlorite matrix (Fig. 4j).
- ***Sample 111.9*** (PDP2c) is a chert vein comprised of dark gray OM-rich chert (Fig. 3g). Up to ~5 vol.% carbonate is present as isolated rhombs of ankerite [23–27 mol.% Fe, Fe/(Fe + Mg) = 0.52–0.59]. The OM in this sample occurs as widespread discrete clots of amorphous shape and variable size, typically 50–200 µm, comprised of a network of nano- to micro-granular OM. Some nano-granular OM is distributed along micro-quartz grain boundaries (Fig. 4k).

To summarize, OM in the Dresser Formation chert/silicified carbonate samples studied include six major microstructure types: clots of amorphous shape and variable size, comprised of nano- to micro-granular OM. The OM clots may be divided into (1) Type-1 clots, which are common in all samples and are of amorphous shape with OM occasionally distributed along micro-quartz grain

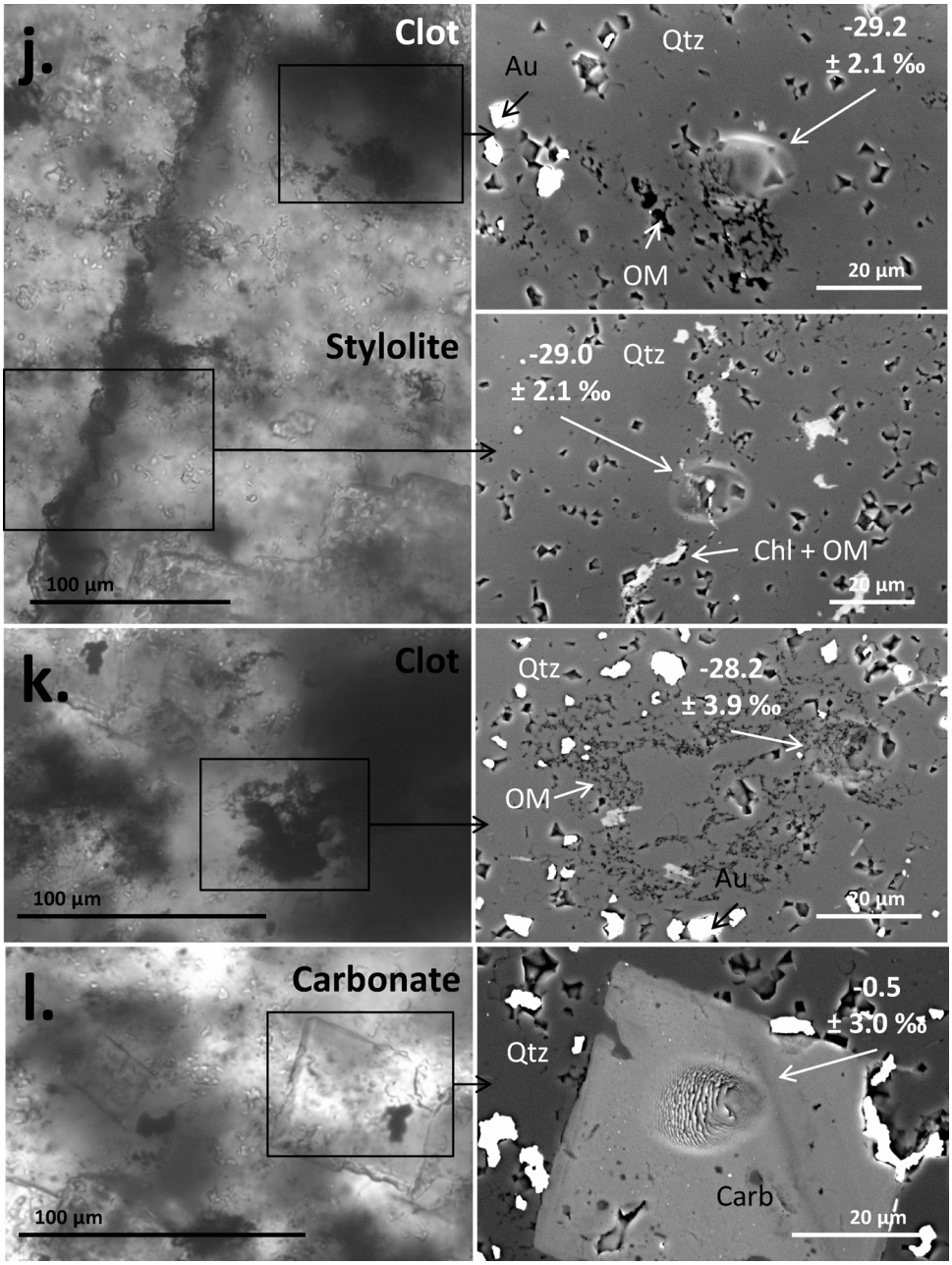

Fig. 4. (*Continued*)

boundaries (e.g. Fig. 4a, e, g, i–k), and (2) Type-2 clots, which are found only in the OM-poor beds of sample 84.4 and are of more distinct shape, sometimes containing concentrated, thread-like OM domains (e.g. Fig. 4b). (3) Layers of sparsely distributed OM comprised of nanometer-scale OM (e.g. Fig. 4c). (4). Fine laminae of nano- to micro-granular OM (e.g. Fig. 4h). (5) OM concentrated along stylolitic fronts, comprised of variable-size chunks of OM often in association with chlorite (e.g. Fig. 4d). (6) OM enclosed in the core of euhedral carbonate rhombs (e.g. Sup. data Fig. S2). The clots (Type-1) are by far the most common OM microstructure occurring in all OM-bearing rocks studied and are sometimes the only OM-microstructure present.

4.2. Carbon isotope data

A total of 97 sample analyses (80 analyses of OM plus 17 analyses of carbonates) and 70 standard analyses (46 analyses of OM plus 24 analyses of carbonates) were performed during the analytical session. The complete SIMS dataset for the studied samples is given in Table 1. For each sample we present the relations between $\delta^{13}C$ values and raw $^{13}CH/^{13}C$ ratios (which serve as a proxy for H/C ratio) of individual OM analysis pits in Fig. 5, and the distribution of $\delta^{13}C(OM)$ values in different OM microstructural types as histograms in Fig. 6. The probabilities associated with Student's *t*-test that two sets of OM $\delta^{13}C$ values, from different samples and/or different microstructural types, come from populations that have the same mean value are summarized in Table 2, together with the absolute difference between the two sets average $\delta^{13}C(OM)$ values. The following section is a detailed description of $\delta^{13}C(OM)$ values in specific OM microstructural types in the different samples.

- 84.4 – Individual spots $\delta^{13}C(OM)$ values in this sample show an overall range of 13.2‰ (−37.6 to −24.4‰) (Fig. 5a). Values of

Table 1
Summary of SIMS session analytical data – samples.

Date	Sample	Spot	Microtexture	$\delta^{13}C_{VPDB}$ (‰)	±2SD[a] (‰)	α_{SIMS}[b]	Bias (‰)	$\delta^{13}C_{RAW}$ (‰)	±2SE[c] (‰)	$^{13}CH/^{13}C$[d]	^{12}C CPS ($\times 10^6$)
6/18/2014	84.4	a1_1a	Stylolite	−25.6	4.6	0.960	−40.31	−64.9	2.3	0.087	1.6
6/18/2014	84.4	a1_1b	Layered	−29.1	4.5	0.960	−40.31	−68.3	2.2	0.077	2.1
6/18/2014	84.4	a1_2a	Layered	−28.2	4.4	0.960	−40.31	−67.3	1.9	0.095	2.1
6/18/2014	84.4	a1_2b	Layered	−26.2	4.3	0.960	−40.31	−65.5	1.7	0.077	2.1
6/18/2014	84.4	a1_3a	Type 1 clot	−26.7	4.1	0.960	−40.31	−65.9	1.1	0.087	4.9
6/18/2014	84.4	a1_4a	Type 1 clot	−27.8	4.1	0.960	−40.31	−67.0	1.2	0.095	5.2
6/18/2014	84.4	a1_5a	Layered	−28.0	6.4	0.960	−40.31	−67.1	4.9	0.148	0.2
6/18/2014	84.4	a1_5b	Layered	−33.5	7.6	0.960	−40.31	−72.5	6.3	0.068	1.1
6/18/2014	84.4	a1_6a	Layered	−32.0	4.5	0.960	−40.31	−71.0	2.1	0.067	1.5
6/18/2014	84.4	a1_6b	Layered	−31.5	4.6	0.960	−40.31	−70.5	2.3	0.087	1.1
6/18/2014	84.4	a6_1a	Type 1 clot	−27.1	4.2	0.960	−40.31	−66.3	1.4	0.084	5.3
6/18/2014	84.4	a6_2a	Type 2 clot	−34.3	4.0	0.960	−40.31	−73.3	0.9	0.083	8.2
6/18/2014	84.4	a7_1a	Stylolite	−24.4	4.2	0.959	−41.10	−64.5	0.9	0.089	7.4
6/18/2014	84.4	a7_1b	Stylolite	−26.2	4.1	0.959	−41.10	−66.2	0.6	0.073	35.9
6/18/2014	84.4	a7_1c	Stylolite	−25.2	4.1	0.959	−41.10	−65.2	0.6	0.072	21.7
6/18/2014	84.4	a7_2a	Stylolite	−27.2	4.1	0.959	−41.10	−67.2	0.6	0.066	27.1
6/18/2014	84.4	a7_2b	Type 1 clot	−27.9	4.5	0.959	−41.10	−67.9	1.8	0.075	3.2
6/18/2014	84.4	a8_4a	Type 1 clot	−28.7	4.3	0.959	−41.10	−68.6	1.2	0.071	5.7
6/18/2014	84.4	a9_2a	Type 2 clot	−29.8	4.2	0.959	−41.10	−69.7	0.8	0.077	12.2
6/18/2014	84.4	a9_3a	Type 2 clot	−31.6	4.2	0.959	−41.10	−71.4	0.8	0.079	13.8
6/18/2014	84.4	a9_4a	Type 2 clot	−37.6	4.2	0.959	−41.10	−77.1	0.8	0.071	9.1
6/18/2014	84.4	a10_1a	Type 2 clot	−34.5	4.2	0.959	−41.10	−74.2	0.9	0.072	14.6
6/18/2014	84.4	a10_1b	Crack	−33.9	4.1	0.959	−41.10	−73.6	0.6	0.128	21.7
6/18/2014	84.4	a10_6a	Type 2 clot	−33.9	4.1	0.959	−41.10	−73.6	0.6	0.064	21.8
6/19/2014	84.5	a3_1a	Clot	−30.2	3.1	0.959	−41.34	−70.3	0.7	0.078	26.2
6/19/2014	84.5	a3_1b	Clot	−32.1	3.1	0.959	−41.34	−72.2	0.5	0.087	27.4
6/19/2014	84.5	a3_2a	Clot	−32.6	3.1	0.959	−41.34	−72.5	0.5	0.081	32.8
6/19/2014	84.5	a3_2b	Clot	−35.7	3.1	0.959	−41.34	−75.6	0.5	0.073	53.0
6/19/2014	84.5	a3_4a	Clot	−32.6	3.2	0.959	−41.34	−72.6	1.0	0.077	7.8
6/19/2014	84.5	a3_4b	Clot	−31.3	3.1	0.959	−41.34	−71.3	0.9	0.096	10.1
6/19/2014	84.5	a3_4c	Carbonate	−1.5	0.7	0.953	−46.90	−48.3	0.4	0.001	30.2
6/19/2014	84.5	a2_2a	No OM	−25.6	4.2	0.959	−41.34	−65.9	3.0	0.079	0.5
6/19/2014	84.5	a2_3a	Clot	−27.2	3.2	0.959	−41.34	−67.4	1.0	0.088	6.2
6/19/2014	84.5	a2_3b	Clot	−30.9	3.1	0.959	−41.34	−71.0	0.7	0.084	13.2
6/18/2014	84.6	a1_1a	Clot	−30.1	2.6	0.958	−41.53	−70.4	0.6	0.100	15.9
6/17/2014	84.6	a1_2a	Clot	−30.0	2.6	0.958	−41.53	−70.3	0.7	0.095	6.8
6/18/2014	84.6	a2_2a	Clot	−26.5	1.6	0.959	−40.91	−66.3	0.8	0.099	12.6
6/18/2014	84.6	a2_3a	Clot	−25.5	1.5	0.959	−40.91	−65.3	0.5	0.103	27.9
6/18/2014	84.6	a2_4a	Clot	−27.6	1.5	0.959	−40.91	−67.4	0.5	0.091	32.2
6/18/2014	84.6	a2_4b	Stylolite	−31.0	2.3	0.959	−40.91	−70.6	1.8	0.136	2.4
6/18/2014	84.6	a2_4c	Clot	−26.8	1.8	0.959	−40.91	−66.6	1.1	0.090	10.0
6/18/2014	84.7	a1_2a	Clot	−26.6	2.6	0.958	−41.53	−67.0	0.5	0.093	49.0
6/18/2014	84.7	a1_3a	Clot	−26.6	2.6	0.958	−41.53	−67.0	0.4	0.098	27.5
6/18/2014	84.7	a1_4a	Clot	−26.6	2.9	0.958	−41.53	−67.0	1.4	0.112	6.8
6/18/2014	84.7	a2_1a	Clot	−29.5	2.6	0.958	−41.53	−69.8	0.6	0.095	13.5
6/18/2014	84.7	a2_2a	Clot	−28.1	2.6	0.958	−41.53	−68.4	0.5	0.101	18.3
6/18/2014	84.7	a2_4a	no OM	−31.6	4.0	0.958	−41.53	−71.8	3.1	0.111	0.6
6/18/2014	84.7	a3_1a	Lamina	−26.1	2.6	0.958	−41.53	−66.6	0.6	0.100	29.8
6/18/2014	84.7	a3_2a	Lamina	−26.0	2.6	0.958	−41.53	−66.5	0.6	0.103	11.9
6/18/2014	84.7	a3_3a	Lamina	−25.7	2.6	0.958	−41.53	−66.1	0.5	0.082	40.8
6/18/2014	84.7	a4_1a	Lamina	−28.5	2.6	0.958	−41.53	−68.8	0.5	0.103	27.7
6/19/2014	84.7	a1_2b	Carbonate	−0.4	3.0	0.954	−46.42	−46.8	0.5	0.004	33.1
6/19/2014	84.7	a1_2c	Carbonate	2.1	3.0	0.954	−46.42	−44.4	0.4	0.002	30.2
6/19/2014	84.7	a1_4b	Carbonate	0.3	3.0	0.954	−46.43	−46.2	0.3	0.004	26.0
6/19/2014	84.7	a2_3a	Carbonate[e]	−9.6	3.0	0.954	−46.43	−55.6	0.5	0.023	48.7
6/19/2014	84.7	a2_3b	Carbonate	0.0	3.0	0.954	−46.39	−46.4	0.4	0.003	30.4
6/19/2014	84.7	a2_3c	Carbonate	−2.2	3.0	0.954	−46.42	−48.5	0.4	0.003	32.4
6/19/2014	93.5a	a3_1a	Clot	−28.3	3.0	0.960	−40.41	−67.6	0.5	0.107	24.2
6/19/2014	93.5a	a3_6a	Clot	−25.8	2.9	0.960	−40.41	−65.1	0.5	0.102	39.4
6/19/2014	93.5a	a3_5a	Clot	−30.0	3.0	0.960	−40.41	−69.2	0.8	0.092	11.5
6/19/2014	93.5a	a3_2a	Clot	−29.3	3.0	0.960	−40.41	−68.6	0.6	0.089	30.5
6/19/2014	93.5b	a1_1a	Clot	−27.0	2.9	0.960	−40.41	−66.3	0.5	0.110	20.8
6/19/2014	93.5b	a1_1b	Clot	−27.5	2.9	0.960	−40.41	−66.8	0.5	0.106	38.7
6/19/2014	93.5b	a1_1c	Layered	−31.8	3.3	0.960	−40.41	−70.9	1.7	0.083	3.1
6/19/2014	93.5b	a1_2a	Clot	−27.3	3.1	0.960	−40.41	−66.6	1.0	0.100	9.7
6/19/2014	93.5b	a1_3a	Clot	−27.1	3.1	0.960	−40.41	−66.4	1.0	0.098	8.0
6/19/2014	93.5b	a1_6a	Layered	−28.5	3.6	0.960	−40.41	−67.8	2.1	0.091	1.3
6/19/2014	93.5b	a1_6b	Layered	−23.6	5.4	0.960	−40.41	−63.1	4.6	0.093	0.3
6/19/2014	93.5b	a1_6c	Layered	−31.5	3.1	0.960	−40.41	−70.6	1.1	0.091	4.5
6/19/2014	93.5b	a2_2a	Clot	−26.9	2.2	0.959	−41.08	−66.9	0.8	0.110	13.3
6/19/2014	93.5b	a2_4a	Stylolite	−28.9	3.6	0.959	−41.08	−68.7	2.9	0.093	1.6
6/19/2014	93.5b	a2_4b	Stylolite	−27.9	2.4	0.959	−41.08	−67.8	1.3	0.094	4.5
6/19/2014	93.5b	a2_5a	Clot	−29.2	2.1	0.959	−41.08	−69.1	0.6	0.096	17.6

Table 1 (*Continued*)

Date	Sample	Spot	Microtexture	$\delta^{13}C_{VPDB}$ (‰)	±2SD[a] (‰)	α_{SIMS}[b]	Bias (‰)	$\delta^{13}C_{RAW}$ (‰)	±2SE[c] (‰)	$^{13}CH/^{13}C$[d]	^{12}C CPS ($\times 10^6$)
6/19/2014	93.5b	a3_2a	Carbonate	−0.1	3.0	0.954	−46.40	−46.5	0.3	0.001	33.3
6/19/2014	93.5b	a3_2b	Clot	−28.2	2.1	0.959	−41.08	−68.1	0.5	0.099	28.2
6/19/2014	93.5b	a3_3a	Clot	−25.9	2.1	0.959	−41.08	−65.9	0.6	0.091	26.0
6/19/2014	93.5b	a2_2b	Carbonate	−0.8	3.0	0.954	−46.40	−47.2	0.4	0.001	30.7
6/19/2014	93.5b	a2_2c	Carbonate	−0.4	3.0	0.954	−46.39	−46.7	0.3	0.001	30.6
6/19/2014	93.5b	a2_5c	Carbonate[e]	−7.5	3.0	0.954	−46.40	−53.6	0.5	0.015	35.8
6/18/2014	111.9	a1_1a	Clot	−26.7	3.9	0.958	−42.06	−67.6	0.5	0.089	30.5
6/18/2014	111.9	a1_1b	Clot	−28.7	3.9	0.958	−42.06	−69.5	0.3	0.082	39.9
6/18/2014	111.9	a1_2a	Clot	−27.9	3.9	0.958	−42.06	−68.8	0.6	0.102	13.3
6/18/2014	111.9	a1_2b	Clot	−30.0	4.1	0.958	−42.06	−70.8	1.3	0.083	3.6
6/18/2014	111.9	a1_3a	Clot	−24.5	3.9	0.958	−42.06	−65.5	0.5	0.113	29.0
6/18/2014	111.9	a1_4a	Clot	−27.2	3.9	0.958	−42.06	−68.1	0.5	0.106	51.7
6/18/2014	111.9	a1_4b	Clot	−27.6	3.9	0.958	−42.06	−68.5	0.6	0.087	19.5
6/18/2014	111.9	a1_5a	Clot	−27.4	3.9	0.958	−42.06	−68.3	0.5	0.103	30.7
6/18/2014	111.9	a2_1a	Clot	−30.8	3.9	0.958	−42.06	−71.6	0.6	0.107	15.3
6/18/2014	111.9	a2_2a	Clot	−28.2	3.9	0.958	−42.06	−69.1	0.5	0.108	33.3
6/18/2014	111.9	a2_3a	Clot	−31.3	4.0	0.958	−42.06	−72.0	1.0	0.082	7.1
6/18/2014	111.9	a2_4a	Clot	−28.9	3.9	0.958	−42.06	−69.7	0.5	0.119	29.4
6/19/2014	111.9	a1_1c	Carbonate	−3.2	3.0	0.954	−46.40	−49.5	0.6	0.005	33.6
6/19/2014	111.9	a1_1d	Carbonate	0.6	3.0	0.954	−46.39	−45.8	0.3	0.002	31.9
6/19/2014	111.9	a1_3b	Carbonate	−0.5	3.0	0.954	−46.41	−46.9	0.3	0.002	31.4
6/19/2014	111.9	a1_3c	Carbonate	−0.8	3.0	0.954	−46.42	−47.2	0.3	0.001	31.5
6/19/2014	111.9	a2_2b	Carbonate	−0.5	3.0	0.954	−46.38	−46.9	0.3	0.001	30.7
6/19/2014	111.9	a2_2c	Carbonate	−1.2	3.0	0.954	−46.41	−47.6	0.3	0.001	29.5

[a] Analytical error is calculated as the quadratic addition of the external precision (calculated as 2SD of $\delta^{13}C$ values from eight bracketing analysis of the PPRG-215-2B std., Sup. data Table S1) and the internal precision for each pit (2SE – see below).

[b] Instrumental bias (α_{SIMS}) is calculated by comparing the average of $d^{13}C_{RAW}$ values for eight bracketing PPRG-215-2B standard analyses (Sup. data Table S1) to the measured bulk value of −31.5‰ (Hayes et al., 1983).

[c] Internal precision (2SE) is calculated as two standard errors of $\delta^{13}C$ values from 80 measurement cycles for each sample analysis pit.

[d] Mass 14 (^{13}CH) was measured simultaneously with ^{12}C and ^{13}C and used to calculate $^{13}CH/^{13}C$.

[e] Post-analysis BSE imaging of this spot suggests that it hit OM enclosed in the carbonate crystal (See Sup. data Fig. S3).

Table 2
Summary of Student's *t*-tests.

	84.4 T1 C	84.4 T2 C	84.4 Lyr	84.4 Stl	84.5 C	84.6 C	84.7 C	84.7 Lam	93.5a C	93.5b C	93.5b Lyr	93.5b Stl	111.9 C
84.4 T1 C		6.0	2.4	1.9	3.9	0.1	0.2	1.1	0.7	0.4	3.0	0.9	0.6
84.4 T2 C	0.00		3.5	7.9	2.0	5.9	6.2	7.0	5.3	6.3	3.0	5.1	5.3
84.4 Lyr	0.08	0.05		4.4	1.5	2.3	2.6	3.5	1.7	2.8	0.5	1.5	1.8
84.4 Stl	0.01	0.00	0.01		5.9	2.0	1.7	0.9	2.6	1.6	4.9	2.8	2.6
84.5 C	0.00	0.16	0.30	0.00		3.8	4.1	5.0	3.2	4.3	1.0	3.0	3.3
84.6 C	0.92	0.00	0.12	0.04	0.01		0.3	1.2	0.6	0.5	2.9	0.8	0.5
84.7 C	0.81	0.00	0.08	0.05	0.01	0.79		0.9	0.9	0.2	3.1	1.1	0.8
84.7 Lam	0.17	0.00	0.05	0.30	0.00	0.33	0.35		1.8	0.7	4.0	2.0	1.7
93.5a C	0.45	0.01	0.31	0.03	0.04	0.62	0.42	0.16		1.1	2.2	0.2	0.1
93.5b C	0.50	0.00	0.05	0.02	0.00	0.55	0.77	0.30	0.19		3.3	1.3	1.0
93.5b Lyr	0.02	0.12	0.78	0.00	0.54	0.07	0.03	0.02	0.17	0.00		2.0	2.3
93.5b Stl	0.13	0.02	0.39	0.01	0.07	0.50	0.23	0.06	0.87	0.06	0.14		0.3
111.9 C	0.48	0.00	0.12	0.01	0.00	0.58	0.40	0.12	0.93	0.16	0.07	0.79	

Below the diagonal black line: The numbers in the boxes show the probability associated with Student's *t*-test that the two sets of OM $\delta^{13}C$ values, from different samples and/or different microstructural types, come from two populations that have the same mean value. Probabilities lower than 0.05 and 0.01 (highlighted in orange and red, respectively) indicate that the two sets are statistically distinct at >95% and >99% confidence level, respectively. Above the diagonal black line: The absolute difference between average $\delta^{13}C$ values for the two sets. Higher values are marked by darker background. *Abbreviations*: C – OM clots; T1 – type 1; T2 – type 2; Lyr – layered OM; Stl – OM in stylolites; Lam – OM laminae.

$\delta^{13}C$(OM) in the Type-1 and Type-2 clots show bimodal distribution with average values of −27.6 and −33.6‰, respectively, which are statistically distinct at >99% confidence level. The Type-2 clots also have distinct $\delta^{13}C$(OM) values (at >95% confidence level) compared to clots in all other samples, excluding sample 84.5, usually being 5–6‰ lower. The layered OM show an intermediate range of $\delta^{13}C$ values, averaging at −30.1‰. OM in the stylolites yielded higher $\delta^{13}C$ values, averaging at −25.7‰, which are statistically distinct at >95% confidence level from all other OM microstructures found in this sample (Fig. 6a; Table 2). The bulk OM $\delta^{13}C$ value of −25.60‰ measured on this sample is similar within the error (2SE) to that found for the stylolites OM (Fig. 6a). This observation is consistent with the massive nature of OM lumps along the stylolitic fronts, which likely comprise most of the OM in this sample.

- 84.5 – The clots in this sample show an approximately normal distribution of $\delta^{13}C$(OM) values with an average of −31.6‰ (Fig. 6b), which is statistically distinct (at >95% confidence level) compared to clots in all other samples, excluding the Type-2 clots in sample 84.4, usually being 3–4‰ lower. The average value of these clots is also lower than the bulk OM $\delta^{13}C$ value of −28.95‰, measured on this sample (Fig. 6b). We note that this sample also contains massive OM lumps within a chlorite matrix along stylolitic fronts, which were not targeted in this study (because of the sample-standard matrix mismatch, as discussed above in Section 4.1). This stylolitic OM may have a lower $\delta^{13}C$ value than associated clots (as seen in sample 84.4) and is more likely to dominate the bulk composition given its massive appearance. One in situ analysis of carbonate by SIMS from this sample yielded a $\delta^{13}C$ value of -1.5 ± 0.7‰.

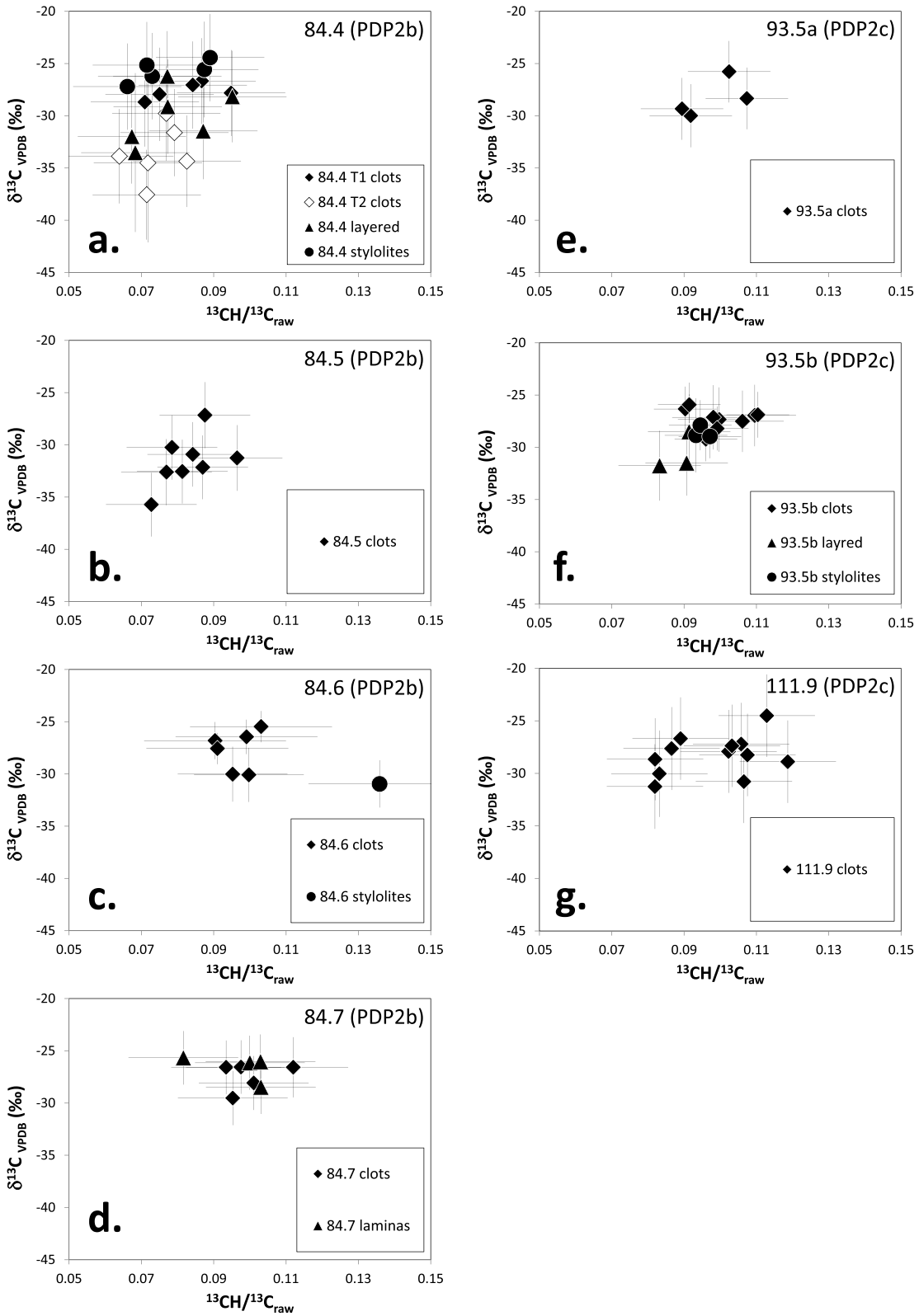

Fig. 5. SIMS $\delta^{13}C$(OM) (‰ VPDB) values plotted vs. raw $^{13}CH/^{13}C$ ratios in the studied samples. The $\delta^{13}C$ and $^{13}CH/^{13}C_{Raw}$ error bars indicate analytical uncertainty as defined in the text.

- 84.6 – The clots in this sample yielded an average $\delta^{13}C$(OM) value of −28.2‰ (Fig. 6c). One analysis of OM in a stylolite yielded $\delta^{13}C$(OM) value of -31.0 ± 2.3‰. However, this value should be treated with caution as the OM in this spot was mostly in chlorite matrix (Sup. data Fig. S3; this is also indicated by higher $^{13}CH/^{13}C$ ratio), for which the instrument mass bias correction may not be applicable.
- 84.7 – Clots and laminated OM in this sample show overlapping distribution of $\delta^{13}C$(OM) values averaging at −27.5 and −26.6‰, respectively, which are statistically indistinct (Fig. 6d; Table 2).

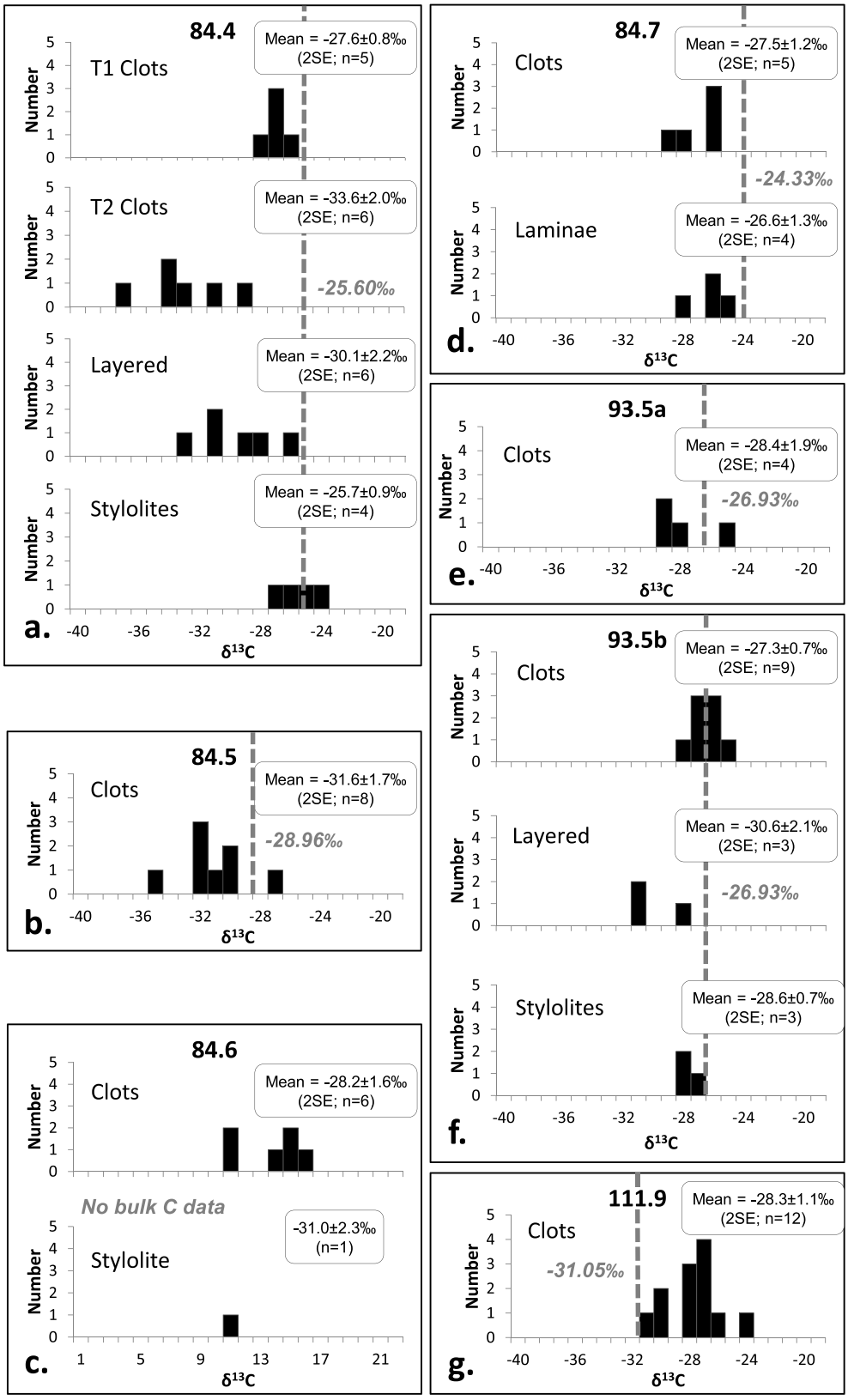

Fig. 6. Histograms of $\delta^{13}C$ values (‰ VPDB) for specific OM microstructures in the studied samples. Dashed gray lines with adjacent numbers in italic indicate the bulk $\delta^{13}C$ values for insoluble OM in each sample.

The average $\delta^{13}C$(OM) of both clots and laminae in this sample, −27.1‰, is slightly lower than the bulk OM $\delta^{13}C$ value of −24.33‰ measured on this sample (Fig. 6d). Five in situ analyses of carbonates from this sample yielded relatively homogeneous $\delta^{13}C$ values with an average of 0.0‰. Another carbonate analysis yielded a much lower value of −9.6‰. However, post-analysis BSE imaging of this spot (84.7_a2_3a) indicates that it hit OM enclosed within the carbonate crystal (Sup. data Fig. S3) and was consequently rejected.

- 93.5a – The clots in this sample yielded an average $\delta^{13}C$(OM) value of −28.4‰ (Fig. 6e).
- 93.5b – Clots and layered OM in this sample show partly overlapping distribution of $\delta^{13}C$(OM) values averaging at −27.3 and −30.6‰, respectively, which are statistically distinct at >95% confidence level. $\delta^{13}C$(OM) values in the stylolites show intermediate distribution with an average of −28.6‰, which is statistically indistinct from those of the clots and the layered OM (Fig. 6f; Table 2). The average $\delta^{13}C$(OM) of all studied microtextures in sample 93.5 ($a+b$), −28.2‰, is slightly lower than the bulk organic OM $\delta^{13}C$ value of −26.95‰ measured on this sample (Fig. 6f). However, the average $\delta^{13}C$(OM) value of the clots, which contain much more OM compared with the layered OM, −27.5‰, is similar within the error (2SE) to the bulk OM value. Three in situ analyses of carbonates from this sample yielded relatively homogeneous $\delta^{13}C$ values with an average of −0.4‰. Another carbonate analysis yielded a notably lower value of −7.5‰. However, post-analysis BSE imaging of this spot (93.5b_a2_5c) suggests that it included OM enclosed within the carbonate crystal (Sup. data Fig. S3) and was consequently rejected.
- 111.9 – The clots in this sample show a relatively large range of raw $^{13}CH/^{13}C$ ratios, between 0.082 and 0.119, but no correlation is seen with $\delta^{13}C$(OM) values (Fig. 5g), which are approximately normally distributed with an average value of −28.3‰. This average value is slightly higher than the bulk OM $\delta^{13}C$ value of −31.05‰, measured in this sample (Fig. 6g). Six in situ analyses of carbonates from this sample yielded relatively homogeneous $\delta^{13}C$ values with an average of −1.0‰.

The total distribution of $\delta^{13}C$(OM) values from this study is presented in Fig. 7 alongside previous $\delta^{13}C$(OM) values reported in the Dresser and the Strelley Pool formations of the Pilbara Craton. The total range of individual in situ $\delta^{13}C$(OM) values found in this work is between −37.6 and −24.4 (quite interestingly, both the highest and lowest values are from the same sample, 84.4), with a prominent concentration of $\delta^{13}C$(OM) values between −29‰ and −26‰ (Fig. 7a). This range of values is wider than that previously reported for the Dresser Formation using bulk OM analysis, −38.3‰ to −29.4‰ (Pinti et al., 2009a; Ueno et al., 2004), and is shifted toward more positive values. However, it is entirely consistent with the range of bulk OM $\delta^{13}C$ values obtained for the samples (Fig. 7e). These differences may thus reflect spatial heterogeneities of OM isotopic compositions within the Dresser Formation. Unlike the samples studied by Ueno et al. (2004), the samples studied here did not show any correlation between TOC content and bulk $\delta^{13}C$(OM) values (Sup. data Table S1). The range of $\delta^{13}C$(OM) values found here is also significantly higher compared to previously reported, graphite-standardized SIMS data for the Dresser Formation OM, which range from −42.3‰ to −30.5‰ (Ueno et al., 2001) (Fig. 7c). The range of $\delta^{13}C$(OM) values obtained here is generally consistent with that obtained using the same methods and calibration standards for the younger Strelley Pool Formation of the Pilbara Craton (−39.9‰ to −25.8‰; Lepot et al., 2013), although the Dresser $\delta^{13}C$(OM) values are skewed toward the lower part of this range whereas the Strelley Pool Formation data show a more even distribution (Fig. 7b). Lepot et al. (2013) carbonaceous chert-standardized SIMS data also show an offset toward higher $\delta^{13}C$ values compared with graphite-standardized SIMS data from the Strelley Pool Formation (−46.0‰ to −32.9‰; Wacey et al., 2011a) (Fig. 7d). This systematic ~7‰ shift of graphite-standardized OM SIMS data toward lower $\delta^{13}C$ values is consistent with the difference in SIMS instrumental bias between graphite (−31‰) and carbonaceous chert (−38‰) reported by House et al. (2000) and a similar trend of increasingly negative bias with higher OM H/C ratio has also been shown by Sangély et al. (2005) and Williford et al. (in press). It is therefore concluded the lower $\delta^{13}C$ values attained from graphite-standardized OM analyses result from erroneous bias correction due to sample-standard matrix mismatch, as discussed in Section 3.2.

5. Discussion

5.1. Primary nature of OM

The OM clots, which occur in all studied samples, are distributed more or less sporadically within the chert/silicified carbonate matrix. There is no network of OM seen connecting the clots and they appear as discrete separated textures. Most of the clots are completely enclosed by micro-crystalline quartz (chert) matrix and are isolated from any mineral-filled veinlets or fissures. The occurrence of similar clots in silicified Archean sediments was interpreted as representing ripped-up microbial mats (Lepot et al., 2013; Tice and Lowe, 2006). Alternatively, bitumen formed by thermal cracking may also polymerize into similar clotted textures. Such "pyrobitumen nodules/globules" are thought to form by rapid maturation during hydrothermal silicification (Buick et al., 1998) or around radioactive mineral grains through radiation-induced polymerization of migrating hydrocarbons (Buick et al., 1998). The OM clots studied here have irregular shape, which is very different from the spherical, smooth-surfaced bitumen globules described in the Warrawoona Group by Buick et al. (1998) and interpreted as oil droplets formed by thermal maturation of older OM during hydrothermal heating. In fact, these bitumen globules coexist with kerogen clots similar to those described here, which are interpreted as the (in situ) bitumen source (Buick et al., 1998). The studied clots also lack any radioactive mineral core as seen in the bitumen nodules formed by immobilization of migrating hydrocarbons (Buick et al., 1998). We therefore interpret the OM clots studied here as primary OM microstructures, such as disrupted microbial mats, or OM that polymerized and/or flocculated in the water column and later settled into the sediment. In some samples, the clots occur mostly or solely within defined OM-rich beds (e.g. samples 84.4 and 84.5; Fig. 3a and b). This bedding of OM clots indicates their early entrainment during sediment deposition, providing additional support to their primary nature (see also Marshall et al., 2007). Likewise, the fine layering/lamination presented by the layered OM and OM laminae (e.g. in samples 84.7 and 93.5b; Fig. 3d and f) indicates their sedimentary origin. Hence, these microstructures are also considered primary OM textures.

Although the OM clots, layers and laminae are considered to be of primary origin, later modification of their OM during diagenesis and hydrothermal/metamorphic alteration is still possible, and might have also overprinted the original isotopic signature. In the following sections we will first evaluate the potential effect of these later processes on the original OM isotopic composition, and then discuss in detail the potential origin(s) of primary OM.

5.2. Alteration of OM

Hydrothermal alteration played an important role during metamorphic overprinting of the North Pole metabasalts and

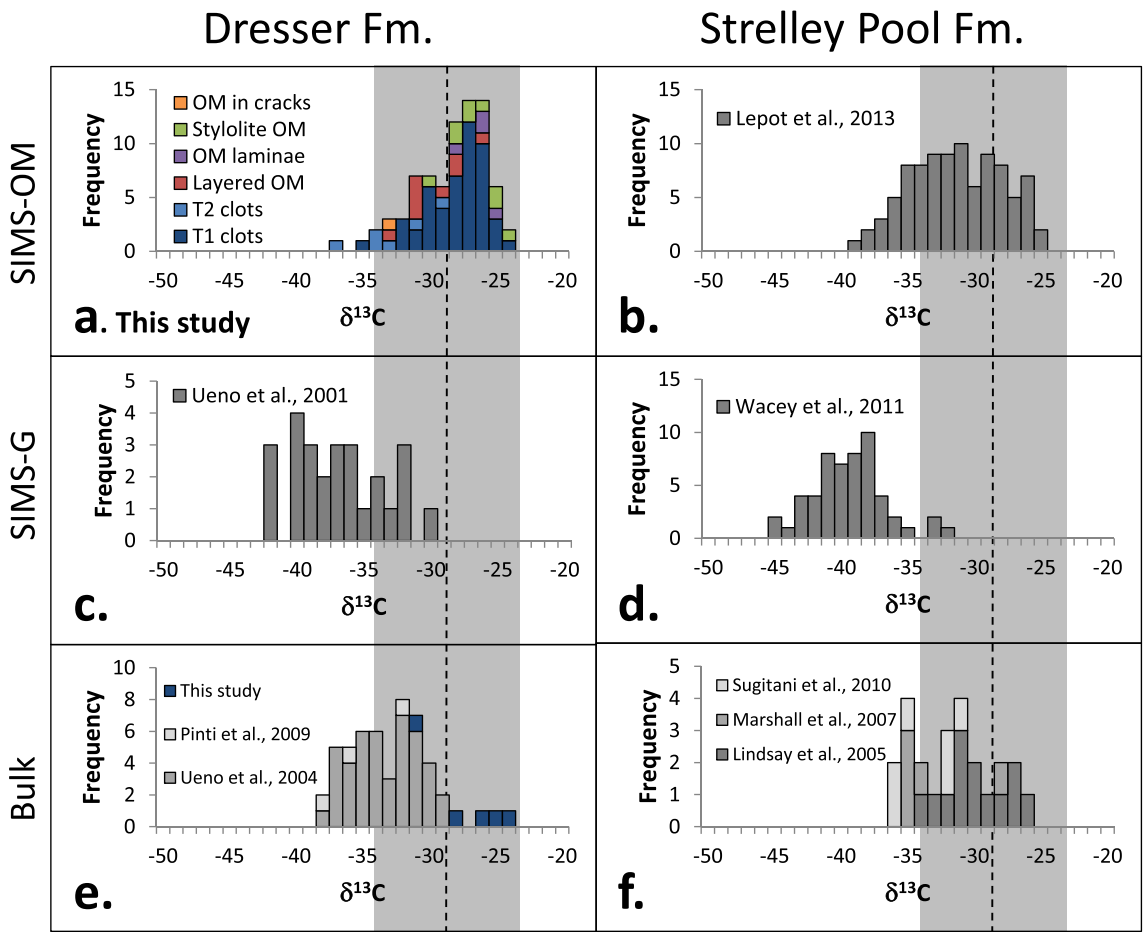

Fig. 7. Summary of OM C-isotope data in the Pilbara Craton from previous work and this study. The data are presented as histograms of $\delta^{13}C$(OM) (‰ VPDB) divided into different formations (Dresser and Strelley Pool) and different analytical methods: a and b–SIMS microanalysis using OM-bearing chert as the calibration standard (SIMS-OM, see text for details); c and d – SIMS microanalysis using graphite as the calibration standard (SIMS-G), e and f – bulk OM analysis (Bulk). The black dashed line indicates the average $\delta^{13}C$ value of all OM analyses in this study and the gray shaded area marks the range included within 2SD.

sedimentary sequence. However, hydrothermal activity is also closely associated with the early stages of deposition of the Dresser Formation bedded chert-barite unit and precipitation of the chert veins. Under these complex circumstances it may be difficult to distinguish early alteration processes taking place during or soon after OM formation, under the same chemical and physical conditions, from later alterations in response to recurring hydrothermal/metamorphic events. Alteration of OM during hydrothermal/metamorphic events could result in modification of its isotopic composition via three main mechanisms: (1) preferential loss of isotopically light carbon compounds during thermal maturation (Des Marais, 2001; Ueno et al., 2004); (2) isotopic exchange with ^{13}C enriched inorganic C, principally from carbonate minerals (Valley, 2001; van Zuilen et al., 2007); and (3) mixing of isotopically variable OM due to OM migration. The possible effects of these processes on the studied samples are discussed below.

5.2.1. *Effect of thermal maturation*

Thermal maturation of OM during diagenesis and/or metamorphism can change the $\delta^{13}C$ value of OM by preferential breaking of the ^{12}C—^{12}C bonds over the ^{12}C—^{13}C bonds, which results in loss of low-$\delta^{13}C$ CH_4 forming a ^{13}C-enriched residue. During this process, OM will also lose heteroatoms such as H, N, O and S, leading to the formation of inverse correlation between $\delta^{13}C$ and H/C-ratio in the residual OM (Des Marais, 2001; Ueno et al., 2004; van Zuilen et al., 2007). This inverse correlation is not seen in any of the samples studied (Fig. 5), indicating that the variability of $\delta^{13}C$(OM) values in our samples is not the result of variable degrees of thermal alteration. Nevertheless, the Dresser OM is typically mature kerogen and may still have been subjected to (uniform) thermal maturation, as suggested by the Raman spectra obtained for a kerogen clot in one of the studied samples (Sup. data Fig. S4), which is similar to that of OM from Alpine metasedimentary rock metamorphosed at ca. 320 °C (Lahfid et al., 2010). Such thermal maturation may have led to the formation of $\delta^{13}C$(OM) values that are slightly higher relative to the original isotopic composition by up to 3‰ (Des Marais, 2001).

5.2.2. *Effect of isotopic exchange*

Isotopic exchange between OM and carbonates mediated by C-bearing fluids could have caused ^{13}C enrichment if hydrothermal/metamorphic alteration was sufficiently intense (e.g. Schidlowski et al., 1983; Ueno et al., 2002; Valley and O'Neil, 1981; Wada and Suzuki, 1983). In the studied bedded chert/carbonate samples, extensive hydrothermal alteration is indicated by the replacement of original sediment by hydrothermal silica and ankerite. This alteration took place at a relatively early stage, during the circulation of hydrothermal fluids that accompanied sediment accumulation (Van Kranendonk et al., 2008). Fluid inclusion data suggest that the bedded cherts at the top of the Dresser Formation were formed from relatively cool aqueous fluid at ~120 °C (Harris et al., 2009). Higher temperatures of about 300–350 °C were recorded in the deeper levels of the hydrothermal system by studies of fluid inclusion and epithermal textures in silica veins (Harris

et al., 2009), and the mineral assemblages in underlying greenstone basalts (Terabayashi et al., 2003). Temperatures of about 300–350 °C are consistent with the Raman spectra obtained for the Dresser OM (Sup. data Fig. S4; Ueno et al., 2004), which are similar to that of OM from lower greenschist facies metasediments (Wopenka and Pasteris, 1993; Yui et al., 1996). While isotopic exchange between organic carbon and carbonate carbon may take place under lower-greenschist facies conditions (Dunn and Valley, 1992), it would have been very sluggish and is unlikely to significantly affect OM isotopic composition, especially in rocks that have undergone earlier silicification, where carbonates where mostly replaced and OM is encased in a quartz matrix. Furthermore, the lack of correlation between the bulk $\delta^{13}C$(OM) value and observed carbonate content in the studied samples supports the absence of substantial isotopic exchange in these samples.

5.2.3. OM migration

Displacement of OM during early hydrothermal alteration of the original carbonate sediment or (re-)crystallization of hydrothermal silica may result in accumulation of OM along grain boundaries, veinlets or voids. This type of small-scale migration of OM has been previously described in the Pilbara Apex chert unit, where it was argued that carbonaceous microfossil-like microstructures were produced by the displacement of (abiologic) OM within a matrix of recrystallizing silica (Brasier et al., 2002, 2005). Distribution of fine-grained OM along microquartz grain boundaries is seen in most of the samples studied, indicating some displacement of OM, probably during silicification of the original carbonate and/or quartz recrystallization. However, this re-distribution of OM is limited to within only a few microns beyond the original clot/layer boundaries. In contrast, OM-rich stylolites suggest OM migration at the mm- to cm-scale. The occurrence of highly concentrated OM along stylolitic fronts in samples 84.4, 84.5 and 93.5b is thought to result from accretion of residual OM following the dissolution of the host carbonate. The occurrence of massive, up to 100 μm thick, chlorite seams along some of the stylolites (Sup. data Fig. S2) suggests their possible relation to later hydrothermal/metamorphic events. However, chlorite can also form during relatively low temperature (130–300 °C) hydrothermal alteration (e.g. Cathelineau and Nieva, 1985) and in some samples scattered chlorite occurs within the chert matrix (84.6, 93.5b; Sup. data Fig. S3). It is therefore possible that chlorite formed before stylolites and was concentrated along the stylolite fronts during host carbonate dissolution, much like the associated OM. In any case, formation of the stylolites (and chlorite) must have occurred at a relatively early stage, prior to, or during silicification of the rock, since they were formed in mostly carbonate matrix. Stylolite OM in sample 93.5b shows an average $\delta^{13}C$ value of −28.6‰, intermediate to that of associated clots (−27.3‰) and layered OM (−30.6‰; Fig. 6f), which can be easily explained by mixture of these components during migration and concentration of OM. However, in sample 84.4 the stylolitic OM, which probably comprises most of the OM in this sample, yielded an average $\delta^{13}C$ value of −25.7‰ (similar to the bulk OM value of −25.60‰) that is heavier than the average $\delta^{13}C$(OM) values of all other studied OM microstructures (Fig. 6a). Therefore, this stylolitic OM isotopic composition cannot be explained by simple mixing of OM from the associated microstructure types. Localized modification of OM along the stylolitic fronts by isotopic exchange with carbonate-bearing fluid formed by enclosing carbonate minerals dissolution (leading to stylolite formation) is possible but suggested to be unlikely due to the relatively low temperatures (<175 °C) experienced by the rocks during early stages of hydrothermal alteration, as discussed above. It is more likely that sediments dissolved during formation of these stylolites included a distinct source of primary OM that had slightly higher $\delta^{13}C$ values compared to that of the studied microstructures.

5.3. Origin of OM

The discussion above has shown that the heterogeneous $\delta^{13}C$ values observed in our samples are probably not the result of later alteration processes and thus represent the complex nature of the primary OM. Processes that may produce such primary $\delta^{13}C$ heterogeneities include variable (biotic and abiotic) organic carbon-fixation paths, biological metabolism and separation of different biomolecule classes with distinct biosynthetic fractionations (Lepot et al., 2013).

Previous evidence for a biogenic origin of the Dresser OM is not conclusive. Dresser OM occurs in bedded silicified carbonates as well as hydrothermal chert veins that formed below the sediment-water interface and it lacks bona fide microfossil structures. Furthermore, the Dresser Formation is dated to ~3.5 Ga, which would make its OM one of the earliest known relicts of life, if indeed biogenic, as claimed by a number of previous authors (e.g. Glikson et al., 2008; Ueno et al., 2004). Supportive of a biogenic origin of the Dresser OM are: the occurrence of putative stromatolites and other microbially-induced sedimentary structures in the Dresser rocks (Noffke et al., 2013; Van Kranendonk et al., 2008), including significant morphological and habitat variations that may indicate diverse communities (Van Kranendonk, 2011); the isotopic signature of sulfur in microscopic sulfide grains (Philippot et al., 2007; Shen et al., 2001; Ueno et al., 2008), which suggest a sulfur-based metabolism for at least some microbes; the relatively low $\delta^{13}C$ values reported for the Dresser OM (Pinti et al., 2009a; Ueno et al., 2004), which are similar to $\delta^{13}C$ values in OM from younger sedimentary rocks of certain biological origin, as well as the magnitude of carbon isotope fractionation between OM and carbonate, which is consistent with that found in modern autotrophic organisms (Ueno et al., 2004 and references therein).

In the following subsections we will examine the potential origins of OM in the Dresser Formation and the importance of later heterotrophic degradation processes using its texture-specific carbon isotope composition in conjunction with previous data regarding possible OM formation processes.

5.3.1. Abiologic origin

Reduced carbonaceous compounds can form abiotically in the natural environment during metamorphic processes such as thermal decomposition of siderite (McCollom, 2003; van Zuilen et al., 2003), reactions between CO_2 and CH_4, or direct reduction of CO_2 in metamorphic fluids (Luque del Villar et al., 1998; Naraoka et al., 1996). Organic compounds might also form by Fischer-Tropsch type (FTT) reactions during hydrothermal alteration of ultramafic rock (Horita and Berndt, 1999; McCollom and Seewald, 2006). This latter process is of particular interest as it has been previously invoked as the source for OM in Pilbara cherts (e.g. Brasier et al., 2002, 2005; Lindsay et al., 2005).

The industrial Fischer Tropsch process uses a metal catalyst to convert carbon monoxide and hydrogen into liquid hydrocarbons. In the geological literature, the term FTT reaction is used more generally to refer to the hydrogenation of inorganic carbon to form organic compounds, often without specifying the nature of the carbon source, the catalyst, the medium in which the reaction occurs or whether the products are volatile or solid (McCollom, 2013). In most cases, dissolved CO_2 is inferred to be the primary carbon source for abiotic organic synthesis in geologic systems. The H_2 required for this reaction might be produced by serpentinization when water circulating through ultramafic rocks forms serpentine and ferrous iron in olivine is altered to ferric iron in magnetite (e.g. McCollom and Bach, 2009; Sleep et al., 2004). Accordingly, FTT synthesis was invoked to explain the emissions of CH_4 observed in some serpentinite-related hydrothermal systems, such as along mid-ocean ridges (e.g. Lost City, Logatchev, and Rainbow

hydrothermal fields in the Atlantic Ocean; Etiope and Schoell, 2014). As the Dresser cherts were deposited/silicified by repeated pulses of hydrothermal fluids that circulated through ultramafic komatiitic basalts (Fig. 2) (Van Kranendonk, 2006), it might be argued that H_2 was present in the hydrothermal fluids, providing the reductant needed for FTT reactions, as suggested for modern mid-ocean ridge environments. However, there is no evidence for extensive serpentinization of the underlying komatiitic basalts, which are completely replaced by a carbonate-white mica–pyrite assemblage, with leucoxene mantling igneous ilmenite (Van Kranendonk et al., 2008). It thus seems that the amount of H_2 present in the Dresser hydrothermal fluids was rather limited. In addition, it is questionable whether appropriate catalysts for FTT reactions existed in the Dresser hydrothermal system. In experimental studies under hydrothermal conditions, FTT synthesis has been demonstrated only in the presence of native metal (Fe-Ni) alloys (McCollom, 2013 and references therein). Reduced metals are exceedingly rare in the crust of the Earth. While the trace occurrence of native metal alloys (Fe, Ni, Cu, Zn and Sn) was mentioned from the Pilbara Apex chert by Brasier et al. (2002) and later by Pinti et al. (2009b, one occurrence), these metals are not documented and have not been verified by other studies of the Dresser Formation cherts (Kozdon et al., 2010; Ueno et al., 2004; Van Kranendonk et al., 2008; this study) and surrounding metavolcanics (Kitajima et al., 2001; Terabayashi et al., 2003). Likewise, these highly reduced phases were probably unstable under the temperatures, redox conditions and sulfide concentrations represented by the chert vein mineral assemblages (Ueno et al., 2004, 2006).

Even if FTT reactions could have taken place within the Dresser hydrothermal system, their potential to produce the amount and type of OM observed in the samples of this study is questionable. In modern serpentinization-related hydrothermal systems where abiotic FTT hydrocarbons formation has been suggested, hydrocarbons occur almost exclusively as methane (Charlou et al., 2002; Proskurowski et al., 2008). In the few places where small amounts of heavier hydrocarbons do occur, they usually consist of simple alkanes from ethane to pentane (e.g. Etiope and Schoell, 2014). These light organic fluids are substantially different from the heavy organic solids (kerogen, bitumen) comprising the Dresser OM (Buick et al., 1998; Ueno et al., 2004) (although methane fluid inclusions have also been reported from Dresser hydrothermal chert veins by Ueno et al., 2006). McCollom and Seewald (2006) have suggested that labile organic compounds could have been synthesized deeper in the hydrothermal system (possibly in the presence of unseen metal catalysts) and subsequently transported to their present location at the upper part of the system, where they have precipitated to form solid organic compounds following conductive cooling or mixing with seawater. Further thermal maturation during metamorphism was also suggested to convert the original organic compounds into their present form (i.e. kerogen). However, we find this scenario inconsistent with the OM distribution, textures and range of $\delta^{13}C$(OM) values reported in this study. Had the OM been formed by precipitation from hydrothermal fluids we would expect to find it mainly in voids and along fissures and not distributed as discreet clots or forming layers and laminae within bedded sediments. Moreover, had the OM been formed entirely by continuous precipitation of simpler hydrocarbons, we would not expect to see any correlation between $\delta^{13}C$(OM) values and specific OM microstructural types as demonstrated in the studied samples. Thus, the in situ carbon isotope data for OM argue strongly against a completely abiotic process.

5.3.2. Biologic origin

All of the samples studied contain rhombs of dolomite-ankerite, whose euhedral form, chemical zoning and the occurrence of quartz inclusions indicate growth during sediment silicification (Fig. 4f and l; Sup. data Fig. S3). In three of the samples, including the chert-vein sample, these ankerites show similar average chemical compositions of ~25 mol.% Fe [Fe/(Fe + Mg) = 0.53–0.55, Sup. data Table S3], as well as similar average $\delta^{13}C$ values of 0‰ to −1‰ (Table 1; Fig. 8). Assuming isotopic equilibrium between dissolved inorganic carbon (DIC) in the precipitating fluids and the ankerites in the samples, the $\delta^{13}C$(Ank) data can be used to estimate the $\delta^{13}C$ of CO_2(aq) in the hydrothermal fluids for a given temperature. While CO_2(aq) may form only part of the total DIC, we focus on this phase as it is the most available for biogenic fixation. If we can assume that OM was formed in hydrothermal fluid similar to those who have precipitated the ankerite, the $\delta^{13}C(CO_2)$ value may be used to calculate the C isotope fractionation between CO_2(aq) and OM [$(\Delta^{13}C(CO_2\text{–OM})$] in the studied samples. We note that making this estimation is not trivial, even when supported by high-spatial-resolution in situ data. Ankerite (and quartz) probably replaced original carbonates in most of the bedded samples and may therefore be late to primary OM formation. Nevertheless, the OM found in the hydrothermal chert vein sample (111.9) probably formed in the hydrothermal fluid. The OM clots in this sample are texturally and isotopically similar to OM clots found in all of the other samples studied suggesting formation in the presence of similar fluids. It was previously suggested that the shallow seafloor environment, where the Dresser bedded sediments were deposited, was dominated by fluids vented from the hydrothermal system (e.g. Harris et al., 2009; Van Kranendonk, 2006; Van Kranendonk and Pirajno, 2004). For the calculation of $\delta^{13}C(CO_2)$ value, we have used the dolomite–CO_2(g) fractionation scheme of Horita (2014) and the CO_2(g)–CO_2(aq) fractionation factor published by Mook et al. (1974). Assuming temperatures in the range of 110–142 °C for the hydrothermal fluids (Harris et al., 2009), CO_2(aq) in equilibrium with the average ankerite isotopic composition would have $\delta^{13}C$ value of between −6‰ and −4‰. These values should be treated with caution as the dolomite–CO_2(g) fractionation was calibrated for dolomite and may differ from that of high-Fe ankerite. However, they provide the best estimate for $\delta^{13}C(CO_2)$ values in the hydrothermal fluids, resulting in $\Delta^{13}C(CO_2\text{–OM})$ of between 20‰ and 30‰ for the studied microstructures. This range of isotopic fractionation is compatible with the range of isotopic fractionation observed in modern autotrophs utilizing the reductive pentose phosphate (Calvin) cycle (mostly photoautotrophs) or the reductive acetyl-CoA pathway (mostly chemolithoautotrophs) (House et al., 2003; Pearson, 2010; Zerkle et al., 2005 and references therein).

Both photosynthesis and chemosynthesis are viable OM-formation processes in the environment represented by the Dresser sediments and veins. The shallow water depth, indicated by the occurrence of ripples, desiccation cracks and the presence of coniform stromatolites (Buick and Dunlop, 1990; Van Kranendonk et al., 2008; Walter et al., 1980), supports the possibility of photoautotrophy, whereas the association with hydrothermal fluids rich in reduced chemical species such as H_2S, Fe^{+2} (Harris et al., 2009; Van Kranendonk, 2006; Van Kranendonk and Pirajno, 2004) and possibly H_2 or CH_4 (as discussed above in Section 5.3.1) suggest that chemolithoautotrophs could have also thrived in this environment. We note that in the Dresser Formation, OM is particularly abundant within the hydrothermal chert veins, which occur below the sediment surface (Ueno et al., 2004). The possibility that OM formed in the water column was introduced in these veins by simple gravitative accumulation in open fissures, or by precipitation of labile or colloidal (i.e. nanoscale) OM circulating through the hydrothermal system, seems less consistent with the higher concentration of OM in the chert veins compared with the bedded sediments (Ueno et al., 2004; Sup. data Table S1). Therefore, it may be concluded that OM was formed in the hydrothermal veins. In this case, the main OM-formation process was probably chemolithoautotrophic production. This conclusion is consistent

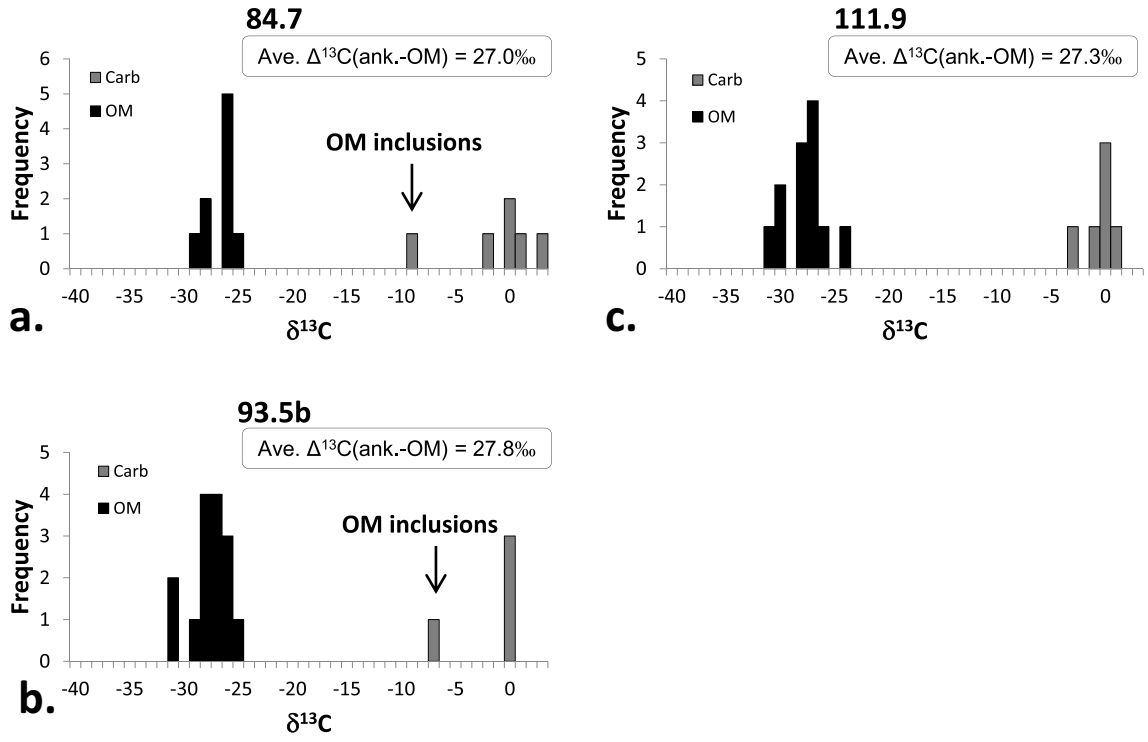

Fig. 8. Histograms of $\delta^{13}C$ (‰ VPDB) values in OM (all microstructures) and ankerites in the studied samples.

with the occurrence of methane with extremely low $\delta^{13}C$ values (< −56‰) in fluid inclusions within the Dresser chert veins that was interpreted as evidence for microbial methanogenesis (Ueno et al., 2006), although the validity of these low $\delta^{13}C(CH_4)$ values as proof for microbial origin have been debated (Etiope and Sherwood Lollar, 2013; Sherwood Lollar and McCollom, 2006). OM in the chert vein sample (111.9) occurs as clots whose morphological appearance and isotopic composition (average −28.3‰) are similar to those of OM clots occurring in all the bedded chert samples, excluding the Type-2 clots in sample 84.4 and the clots in sample 84.5, which yielded significantly lower $\delta^{13}C(OM)$ values (Table 2). This may imply that chemolithoautotrophic production was the main OM formation process also in the bedded cherts. Nevertheless, the occurrence of stromatolites in the Dresser Formation sediments is more consistent with photoautotrophic organisms (Van Kranendonk, 2011; Walter et al., 1980). We also note that the overall range of $\delta^{13}C(OM)$ values found in the Dresser Formation is similar to that reported for the younger (~3.4 Ga) Strelley Pool Formation of the Pilbara Craton (Lepot et al., 2013) (Fig. 7), which is widely regarded as containing photoautotrophic stromatolites (e.g. Allwood et al., 2007). A simplified model of the earliest-known inhabited environment on Earth may therefore be considered, where H_2S, Fe^{2+} and possibly H_2 and CH_4 are continuously being produced by hydrothermal circulation through the young basaltic crust, providing electron donors for both chemolithoautotrophs and anoxygenic photoautotrophs. A similar scenario has also been proposed for younger (3.2–3.4 Ga) early Archean OM-bearing cherts of the Barberton Greenstone Belt in South Africa (van Zuilen et al., 2007). Accordingly, the heterogeneous $\delta^{13}C(OM)$ values reported here for some of the Dresser bedded chert/carbonate samples may be explained by different organisms utilizing different C-fixation paths. Alternatively, differences in $\delta^{13}C(OM)$ values may represent changes in $\Delta^{13}C(CO_2\text{-}OM)$ arising from changes in the availability of CO_2 for the autotrophic organisms. Rapid growth of microbial communities in conjunction with restricted permeability in the sediments, or pulsed fluid flow in hydrothermal conduits may limit the amount of CO_2 in these environments. This may result in consumption of a larger fraction of the dissolved CO_2 leading to smaller $\Delta^{13}C(CO_2\text{-}OM)$ values (e.g. Deuser et al., 1968; Calder and Parker, 1973). Shifts in the magnitude of $\Delta^{13}C(CO_2\text{-}OM)$ in methanogens were also shown to occur during growth of the organism communities, as a function of cell density (House et al., 2003).

The range of values observed in the samples may also be explained by separation of different classes of biomolecules from the biomass of a single autotrophic organism, as well as from the biomass of a complex ecosystem (Hayes, 2001; Pearson, 2010). Biosynthetic processes within a single cell form micro-reservoirs comprised of different classes of organic molecules, which may have $\delta^{13}C(OM)$ values distinct from that of the whole cell (Hayes, 2001; Sakata et al., 1997; Teece and Fogel, 2007). These distinct micro-reservoirs can sometimes be distinguished by in situ $\delta^{13}C(OM)$ analysis of well-preserved microfossils as shown by Williford et al. (2013). These classes of molecules have distinct reactivity and may polymerize separately during early degradation and diagenesis processes (Close et al., 2011; Damsté et al., 1998; Galimov, 2006; Williford et al., 2013). Nevertheless, we have found no correlation between average $\delta^{13}C(OM)$ values and H/C ratio in the different microstructures studied here suggesting that the microstructure-specific isotopic compositions do not result from condensation and/or preservation of specific classes of biomolecules.

Glikson et al. (2008) have compared the OM preserved in the Dresser cherts with the remains of modern hyperthermophilic methanogens from an active seafloor hydrothermal environment using organic petrography, transmission electron microscopy (TEM) and SEM coupled with energy-dispersive X-ray spectroscopy (EDS). These authors report considerable morphological and textural similarity between the Dresser OM and the thermally degraded remains of the organism formed after heating the cultures to >100 °C, which resulted in disintegration of most cellular structures. It is likely that the OM clots abundant in the samples studied here represent a similarly degraded form of the original OM.

Morphologically similar OM clots from the Strelley Pool Formation were also described as a polymerized residue of degraded microbial OM (Lepot et al., 2013). Glikson et al. (2008) have suggested that thermal degradation of primary OM in the Dresser samples resulted in higher $\delta^{13}C$(OM) values due to preferential loss of low-$\delta^{13}C$ CH_4. However, this process is expected to result in correlated lower H/C ratios with higher $\delta^{13}C$, which are not observed in any of our samples, as discussed above in Section 5.1 and shown in Fig. 5. Heterotrophic degradation on the other hand is also capable of increasing OM $\delta^{13}C$ by a few permil (Pearson, 2010), but without necessarily producing a distinct correlation with OM H/C ratio. Therefore, the range of $\delta^{13}C$(OM) values in the Dresser samples may also arise, at least partly, due to the effect of variable heterotrophic degradation. A similar process has been invoked to explain the higher than bulk-rock $\delta^{13}C$ values found in situ for some of the OM clots in the Strelley Pool Formation samples studied by Lepot et al. (2013). Yet, unlike in the Strelley Pool Formation, where pristine OM microstructures such as lenses and spheres have been preserved, it seems that in the Dresser Formation samples studied here, all cellular textures were degraded to form amorphous OM clots. Nevertheless, we note that some of the Type-2 clots of sample 84.4, which yielded the lowest $\delta^{13}C$(OM) values in this study, comprise thread-like portions of denser OM (e.g. 84.4_a9_4a; Fig. 4b), which may represent a more pristine, less degraded form of the original autotrophic OM.

6. Conclusions

1. Through petrographic study of the Dresser Formation cherts we have described six distinct OM microstructural types: OM clots, which may be subdivided into Type-1 and -2 clots, layered OM, laminated OM, OM concentrated along stylolites and OM enclosed in carbonate rhombs. Our study identifies most of the OM microstructures in these rocks as indigenous and syngenetic, formed within unconsolidated sediments or hydrothermal veins during their deposition/precipitation. Later migration of OM within the rocks during hydrothermal/metamorphic alteration events occurred over a very limited, micrometer scale, or is confined along distinct stylolitic fronts formed by the dissolution of primary carbonate, prior to silicification.
2. Average $\delta^{13}C$(OM) values in the studied microstructural types range between −33.6‰ and −25.7‰. Thermal maturation or isotope exchange reactions with C-bearing fluids probably did not significantly alter the original $\delta^{13}C$ value of OM as is indicated by the lack of a negative correlation between $\delta^{13}C$ values and H/C ratios in OM, and the relatively low temperature alteration of the host rock. It is thus concluded that the ~7‰ range of average $\delta^{13}C$(OM) values found for the studied microstructures represents primary variability in OM isotopic composition.
3. Some of the samples studied show a relatively wide range of $\delta^{13}C$(OM) values, which correlate to microstructure types. This observation is not consistent with the hypothesis that all OM formed by precipitation of abiotically formed simple organic compounds. Likewise, there is no evidence that hydrogen, required as a source of reduction in most abiotic hydrocarbon-forming reactions, was present in the hydrothermal fluids and the native metal alloys required as catalysts for abiotic FFT reactions were not detected in the rocks studied here or in nearby metabasalts.
4. Average $\Delta^{13}C(CO_2\text{–OM})$ values obtained in this study for different OM microstructure types range between 20‰ and 30‰. This range of isotopic fractionation is consistent with enzymatic C fixation via the Calvin cycle utilized by photoautotrophs and the reductive acetyl-CoA pathway utilized by chemolithoautotrophs. Photoautotrophy is suggested by the relatively shallow water depth inferred for the Dresser environment and the occurrence of stromatolites in this unit, whereas chemolithotrophy is supported by the abundance of OM in the chert veins that are interpreted as sub-surface hydrothermal conduits. Therefore, the range of $\delta^{13}C$(OM) values observed in some of the Dresser Formation samples may be explained by different primary OM formation paths. The observed $\delta^{13}C$(OM) heterogeneities may also reflect other biogenic processes, such as differences in biomass density and heterotrophic overprinting of the primary (i.e. autotrophic) OM.

Acknowledgements

We thank Noriko Kita and Jim Kern for assistance with the ion microprobe, John Fournelle and Phil Gopon for assistance with the SEM and EPMA, Maciej Śliwiński for assistance with the carbonate SIMS standards and data processing, and Brian Hess for expert sample preparation. Chris House provided our standard chip of PPRG-215. Funding for this study was provided by the NASA Astrobiology Institute (NM, KW, KK, KL, JV) and the Labex UnivEarths program of Sorbonne Paris Cité (ANR-10-LABX-0023 and ANR-11-IDEX-0005-02, PP, KL, CT). Work by KW at the Jet Propulsion Laboratory, California Institute of Technology was funded by a grant from the National Aeronautics and Space Administration. MVK acknowledges support from the University of New South Wales. The WiscSIMS Lab is partly supported by NSF-EAR-1053466, -1355590. Drillcore samples were made available through the collaborative PDP drilling project organized by the Institute de Physique de Globe de Paris and the Geological Survey of Western Australia. This is contribution 699 from the Australian Research Council Centre of Excellence for Core to Crust Fluid Systems.

Appendix A. Supplementary data

Supplementary data associated with this article can be found, in the online version, at http://dx.doi.org/10.1016/j.precamres.2016.01.014.

References

Allwood, A.C., Walter, M.R., Burch, I.W., Kamber, B.S., 2007. 3.43 billion-year-old stromatolite reef from the Pilbara Craton of Western Australia: ecosystem-scale insights to early life on Earth. Precambrian Res. 158, 198–227.
Amelin, Y., Lee, D.-C., Halliday, A., 2000. Early-middle Archaean crustal evolution deduced from Lu-Hf and U-Pb isotopic studies of single zircon grains. Geochim. Cosmochim. Acta 64, 4205–4225.
Awramik, S., Schopf, J., Walter, M., 1983. Filamentous fossil bacteria from the Archean of Western Australia. Precambrian Res. 20, 357–374.
Brasier, M.D., Green, O.R., Jephcoat, A.P., Kleppe, A.K., Van Kranendonk, M.J., Lindsay, J.F., Steele, A., Grassineau, N.V., 2002. Questioning the evidence for Earth's oldest fossils. Nature 416, 76–81.
Brasier, M.D., Green, O.R., Lindsay, J.F., McLoughlin, N., Steele, A., Stoakes, C., 2005. Critical testing of Earth's oldest putative fossil assemblage from the ~3.5 Ga Apex chert, Chinaman Creek, Western Australia. Precambrian Res. 140, 55–102.
Buick, R., 1984. Carbonaceous filaments from North Pole, Western Australia: are they fossil bacteria in Archaean stromatolites? Precambrian Res. 24, 157–172.
Buick, R., 1990. Microfossil recognition in Archean rocks: an appraisal of spheroids and filaments from a 3500 my old chert-barite unit at North Pole, Western Australia. Palaios, 441–459.
Buick, R., Dunlop, J., 1990. Evaporitic sediments of early Archaean age from the Warrawoona Group, North Pole, Western Australia. Sedimentology 37, 247–277.
Buick, R., Dunlop, J., Groves, D., 1981. Stromatolite recognition in ancient rocks: an appraisal of irregularly laminated structures in an Early Archaean chert-barite unit from North Pole, Western Australia. Alcheringa 5, 161–181.
Buick, R., Rasmussen, B., Krapez, B., 1998. Archean oil: evidence for extensive hydrocarbon generation and migration 2.5–3.5 Ga. AAPG Bull. 82, 50–69.
Calder, J.A., Parker, P.L., 1973. Geochemical implications of induced changes in C^{13} fractionation by blue-green algae. Geochim. Cosmochim. Acta 37, 133–140.
Cathelineau, M., Nieva, D., 1985. A chlorite solid solution geothermometer the Los Azufres (Mexico) geothermal system. Contrib. Mineral. Petrol. 91, 235–244.
Charlou, J., Donval, J., Fouquet, Y., Jean-Baptiste, P., Holm, N., 2002. Geochemistry of high H_2 and CH_4 vent fluids issuing from ultramafic rocks at the Rainbow hydrothermal field (36°14′ N. MAR). Chem. Geol. 191, 345–359.

Close, H., Bovee, R., Pearson, A., 2011. Inverse carbon isotope patterns of lipids and kerogen record heterogeneous primary biomass. Geobiology 9, 250–265.
Damsté, J.S.S., Kok, M.D., Köster, J., Schouten, S., 1998. Sulfurized carbohydrates: an important sedimentary sink for organic carbon? Earth Planet. Sci. Lett. 164, 7–13.
Des Marais, D.J., 2001. Isotopic evolution of the biogeochemical carbon cycle during the Precambrian. Rev. Mineral. Geochem. 43, 555–578.
Deuser, W.G., Degens, E.T., Guillard, R.R.L., 1968. Carbon isotope relationships between plankton and sea water. Geochim. Cosmochim. Acta 32, 657–660.
Dunn, S., Valley, J.W., 1992. Calcite–graphite isotope thermometry: a test for polymetamorphism in marble, Tudor gabbro aureole, Ontario, Canada. J. Metamorph. Geol. 10, 487–501.
Eiler, J.M., Graham, C., Valley, J.W., 1997. SIMS analysis of oxygen isotopes: matrix effects in complex minerals and glasses. Chem. Geol. 138, 221–244.
Etiope, G., Schoell, M., 2014. Abiotic gas: atypical, but not rare. Elements 10, 291–296.
Etiope, G., Sherwood Lollar, B., 2013. Abiotic methane on earth. Rev. Geophys. 51, 276–299.
Foriel, J., Philippot, P., Rey, P., Somogyi, A., Banks, D., Ménez, B., 2004. Biological control of Cl/Br and low sulfate concentration in a 3.5-Gyr-old seawater from North Pole, Western Australia. Earth Planet. Sci. Lett. 228, 451–463.
Galimov, E., 2006. Isotope organic geochemistry. Org. Geochem. 37, 1200–1262.
Glikson, M., Duck, L.J., Golding, S.D., Hofmann, A., Bolhar, R., Webb, R., Baiano, J.C., Sly, L.I., 2008. Microbial remains in some earliest Earth rocks: comparison with a potential modern analogue. Precambrian Res. 164, 187–200.
Harris, A.C., White, N.C., McPhie, J., Bull, S.W., Line, M.A., Skrzeczynski, R., Mernagh, T.P., Tosdal, R.M., 2009. Early Archean hot springs above epithermal veins, North Pole, Western Australia: new insights from fluid inclusion microanalysis. Econ. Geol. 104, 793–814.
Hayes, J.M., 2001. Fractionation of carbon and hydrogen isotopes in biosynthetic processes. In: Valley, J.W., Cole, D. (Eds.), Stable isotope Geochemistry, Mineralogical Society of America. Rev. Mineral. Geochem. 43, 225–277.
Hayes, J.M., Kaplan, I.R., Wedeking, K.W., 1983. Precambrian organic geochemistry, preservation of the record. In: Schopf, J.W. (Ed.), Earth's Earliest Biosphere. Princeton University Press, pp. 93–134.
Hickman, A.H., 1983. Geology of the Pilbara Block and its Environs. Geological Survey of Western Australia, Perth, Western Australia.
Horita, J., 2014. Oxygen and carbon isotope fractionation in the system dolomite–water–CO_2 to elevated temperatures. Geochim. Cosmochim. Acta 129, 111–124.
Horita, J., Berndt, M.E., 1999. Abiogenic methane formation and isotopic fractionation under hydrothermal conditions. Science 285, 1055–1057.
House, C.H., Schopf, J.W., McKeegan, K.D., Coath, C.D., Harrison, T.M., Stetter, K.O., 2000. Carbon isotopic composition of individual Precambrian microfossils. Geology 28, 707–710.
House, C.H., Schopf, J.W., Stetter, K.O., 2003. Carbon isotopic fractionation by Archaeans and other thermophilic prokaryotes. Org. Geochem. 34, 345–356.
Huberty, J.M., Kita, N.T., Kozdon, R., Heck, P.R., Fournelle, J.H., Spicuzza, M.J., Xu, H., Valley, J.W., 2010. Crystal orientation effects in $\delta^{18}O$ for magnetite and hematite by SIMS. Chem. Geol. 276, 269–283.
Isozaki, Y., Kabashima, T., Ueno, Y., Kitajima, K., Maruyama, S., Kato, Y., Terabayashi, M., 1997. Early Archean mid-oceanic ridge rocks and early life in the Pilbara Craton, W. Australia. Eos 78, 399.
Kita, N.T., Ushikubo, T., Fu, B., Valley, J.W., 2009. High precision SIMS oxygen isotope analysis and the effect of sample topography. Chem. Geol. 264, 43–57.
Kitajima, K., Maruyama, S., Utsunomiya, S., Liou, J., 2001. Seafloor hydrothermal alteration at an Archaean mid-ocean ridge. J. Metamorph. Geol. 19, 583–599.
Kozdon, R., Kita, N.T., Huberty, J.M., Fournelle, J.H., Johnson, C.A., Valley, J.W., 2010. *In situ* sulfur isotope analysis of sulfide minerals by SIMS: precision and accuracy, with application to thermometry of ~3.5 Ga Pilbara cherts. Chem. Geol. 275, 243–253.
Lahfid, A., Beyssac, O., Deville, E., Negro, F., Chopin, C., Goffé, B., 2010. Evolution of the Raman spectrum of carbonaceous material in low-grade metasediments of the Glarus Alps (Switzerland). Terra Nova 22, 354–360.
Lepot, K., Williford, K.H., Ushikubo, T., Sugitani, K., Mimura, K., Spicuzza, M.J., Valley, J.W., 2013. Texture-specific isotopic compositions in 3.4 Gyr old organic matter support selective preservation in cell-like structures. Geochim. Cosmochim. Acta 112, 66–86.
Lindsay, J., Brasier, M., McLoughlin, N., Green, O., Fogel, M., Steele, A., Mertzman, S., 2005. The problem of deep carbon – an Archean paradox. Precambrian Res. 143, 1–22.
Luque del Villar, F.J., Pasteris, J.D., Wopenka, B., Rodas, M., Fernández Barrenechea, J.M., 1998. Natural fluid-deposited graphite: mineralogical characteristics and mechanisms of formation. Am. J. Sci. 298, 471–498.
Marshall, A.O., Emry, J.R., Marshall, C.P., 2012. Multiple generations of carbon in the Apex Chert and implications for preservation of microfossils. Astrobiology 12, 160–166.
Marshall, C.P., Love, G.D., Snape, C.E., Hill, A.C., Allwood, A.C., Walter, M.R., Van Kranendonk, M.J., Bowden, S.A., Sylva, S.P., Summons, R.E., 2007. Structural characterization of kerogen in 3.4 Ga Archaean cherts from the Pilbara Craton, Western Australia. Precambrian Res. 155, 1–23.
McCollom, T.M., 2003. Formation of meteorite hydrocarbons from thermal decomposition of siderite ($FeCO^3$). Geochim. Cosmochim. Acta 67, 311–317.
McCollom, T.M., 2013. Laboratory simulations of abiotic hydrocarbon formation in Earth's deep subsurface. In: Hazen, R.M., Jones, A.P., Baross, J.A. (Eds.), Carbon in Earth, Mineralogical Society of America. Rev. Mineral. Geochem. 75, 467–494.
McCollom, T.M., Bach, W., 2009. Thermodynamic constraints on hydrogen generation during serpentinization of ultramafic rocks. Geochim. Cosmochim. Acta 73, 856–875.
McCollom, T.M., Seewald, J.S., 2006. Carbon isotope composition of organic compounds produced by abiotic synthesis under hydrothermal conditions. Earth Planet. Sci. Lett. 243, 74–84.
McKeegan, K.D., Walker, R.M., Zinner, E., 1985. Ion microprobe isotopic measurements of individual interplanetary dust particles. Geochim. Cosmochim. Acta 49, 1971–1987.
Mook, W., Bommerson, J., Staverman, W., 1974. Carbon isotope fractionation between dissolved bicarbonate and gaseous carbon dioxide. Earth Planet. Sci. Lett. 22, 169–176.
Naraoka, H., Ohtake, M., Maruyama, S., Ohmoto, H., 1996. Non-biogenic graphite in 3.8-Ga metamorphic rocks from the Isua district, Greenland. Chem. Geol. 133, 251–260.
Nijman, W., de Bruijne, K., Valkering, M.E., 1999. Growth fault control of Early Archaean cherts, barite mounds and chert-barite veins, North Pole Dome, Eastern Pilbara, Western Australia. Precambrian Res. 95, 247–274.
Noffke, N., Christian, D., Wacey, D., Hazen, R.M., 2013. Microbially induced sedimentary structures recording an ancient ecosystem in the ca. 3.48 billion-year-old Dresser Formation, Pilbara, Western Australia. Astrobiology 13, 1103–1124.
Pearson, A., 2010. Pathways of carbon assimilation and their impact on organic matter values $\delta^{13}C$. In: Timmis, K.N. (Ed.), Handbook of Hydrocarbon and Lipid Microbiology. Springer-Verlag, Berlin Heidelberg, pp. 144–156.
Philippot, P., Van Zuilen, M., Lepot, K., Thomazo, C., Farquhar, J., Van Kranendonk, M.J., 2007. Early Archaean microorganisms preferred elemental sulfur, not sulfate. Science 317, 1534–1537.
Pinti, D.L., Hashizume, K., Sugihara, A., Massault, M., Philippot, P., 2009a. Isotopic fractionation of nitrogen and carbon in Paleoarchean cherts from Pilbara craton, Western Australia: origin of ^{15}N-depleted nitrogen. Geochim. Cosmochim. Acta 73, 3819–3848.
Pinti, D.L., Mineau, R., Clement, V., 2009b. Hydrothermal alteration and microfossil artefacts of the 3465-million-year-old Apex chert. Nat. Geosci. 2, 640–643.
Proskurowski, G., Lilley, M.D., Seewald, J.S., Früh-Green, G.L., Olson, E.J., Lupton, J.E., Sylva, S.P., Kelley, D.S., 2008. Abiogenic hydrocarbon production at Lost City hydrothermal field. Science 319, 604–607.
Sakata, S., Hayes, J.M., McTaggart, A.R., Evans, R.A., Leckrone, K.J., Togasaki, R.K., 1997. Carbon isotopic fractionation associated with lipid biosynthesis by a cyanobacterium: relevance for interpretation of biomarker records. Geochim. Cosmochim. Acta 61, 5379–5389.
Sangély, L., Chaussidon, M., Michels, R., Huault, V., 2005. Microanalysis of carbon isotope composition in organic matter by secondary ion mass spectrometry. Chem. Geol. 223, 179–195.
Schidlowski, M., Hayes, J., Kaplan, I., 1983. Isotopic inferences of ancient biochemistries – carbon, sulfur, hydrogen, and nitrogen. In: Schopf, J.W. (Ed.), The Earth's Earliest Biosphere. Princeton University Press, Princeton, New Jersey, pp. 149–185.
Shen, Y., Buick, R., Canfield, D.E., 2001. Isotopic evidence for microbial sulphate reduction in the early Archaean era. Nature 410, 77–81.
Sherwood Lollar, B., McCollom, T.M., 2006. Geochemistry: biosignatures and abiotic constraints on early life. Nature 444, E18.
Sleep, N., Meibom, A., Fridriksson, T., Coleman, R., Bird, D., 2004. H_2-rich fluids from serpentinization: geochemical and biotic implications. Proc. Natl. Acad. Sci. U. S. A. 101, 12818–12823.
Śliwiński, M.G., Kitajima, K., Kozdon, R., Spicuzza, M.J., Fournelle, J., Denny, A., Valley, J.W., 2015. Secondary ion mass spectrometry bias on isotope ratios in dolomite–ankerite, Part II: $\delta^{13}C$ matrix effects. Geostand. Geoanal. Res. (in press).
Teece, M.A., Fogel, M.L., 2007. Stable carbon isotope biogeochemistry of monosaccharides in aquatic organisms and terrestrial plants. Org. Geochem. 38, 458–473.
Terabayashi, M., Masada, Y., Ozawa, H., 2003. Archean ocean-floor metamorphism in the North Pole area, Pilbara Craton, Western Australia. Precambrian Res. 127, 167–180.
Tessalina, S.G., Bourdon, B., Van Kranendonk, M., Birck, J.-L., Philippot, P., 2010. Influence of Hadean crust evident in basalts and cherts from the Pilbara Craton. Nat. Geosci. 3, 214–217.
Thorpe, R., Hickman, A., Davis, D., Mortensen, J., Trendall, A., 1992a. Constraints to models for Archaean lead evolution from precise zircon U–Pb geochronology for the Marble Bar region, Pilbara Craton, Western Australia. Archaean: Terrains Process. Metallog., 395–407.
Thorpe, R., Hickman, A., Davis, D., Mortensen, J., Trendall, A., 1992b. U-Pb zircon geochronology of Archaean felsic units in the Marble Bar region, Pilbara Craton, Western Australia. Precambrian Res. 56, 169–189.
Tice, M.M., Lowe, D.R., 2006. The origin of carbonaceous matter in pre-3.0 Ga greenstone terrains: a review and new evidence from the 3.42 Ga Buck Reef Chert. Earth-Sci. Rev. 76, 259–300.
Ueno, Y., Isozaki, Y., Yurimoto, H., Maruyama, S., 2001. Carbon isotopic signatures of individual Archean microfossils (?) from Western Australia. Int. Geol. Rev. 43, 196–212.
Ueno, Y., Ono, S., Rumble, D., Maruyama, S., 2008. Quadruple sulfur isotope analysis of ca. 3.5 Ga Dresser Formation: new evidence for microbial sulfate reduction in the early Archean. Geochim. Cosmochim. Acta 72, 5675–5691.
Ueno, Y., Yamada, K., Yoshida, N., Maruyama, S., Isozaki, Y., 2006. Evidence from fluid inclusions for microbial methanogenesis in the early Archaean era. Nature 440, 516–519.

Ueno, Y., Yoshioka, H., Maruyama, S., Isozaki, Y., 2004. Carbon isotopes and petrography of kerogens in ~3.5-Ga hydrothermal silica dikes in the North Pole area, Western Australia. Geochim. Cosmochim. Acta 68, 573–589.

Ueno, Y., Yurimoto, H., Yoshioka, H., Komiya, T., Maruyama, S., 2002. Ion microprobe analysis of graphite from ca. 3.8 Ga metasediments, Isua supracrustal belt, West Greenland: relationship between metamorphism and carbon isotopic composition. Geochim. Cosmochim. Acta 66, 1257–1268.

Valley, J., O'Neil, J.R., 1981. $^{13}C/^{12}C$ exchange between calcite and graphite: a possible thermometer in Grenville marbles. Geochim. Cosmochim. Acta 45, 411–419.

Valley, J.W., 2001. Stable isotope thermometry at high temperatures. In: Valley, J.W., Cole, D. (Eds.), Stable isotope Geochemistry, Mineralogical Society of America. Rev. Mineral. Geochem. 43, 365–414.

Valley, J.W., Kita, N.T., 2009. In situ oxygen isotope geochemistry by ion microprobe. MAC Short Course: Secondary Ion Mass Spectrometry in the Earth Sciences, vol. 41., pp. 19–63.

Van Kranendonk, M., 2011. Stromatolite morphology as an indicator of biogenicity for Earth's oldest fossils from the 3.5–3.4 Ga Pilbara Craton, Western Australia. Advances in Stromatolite Geobiology. Lecture Notes in Earth Sciences, vol. 131., pp. 517–534.

Van Kranendonk, M.J., 2006. Volcanic degassing, hydrothermal circulation and the flourishing of early life on Earth: a review of the evidence from c. 3490–3240 Ma rocks of the Pilbara Supergroup, Pilbara Craton, Western Australia. Earth-Sci. Rev. 74, 197–240.

Van Kranendonk, M.J., 2010. Three and a half billion years of life on Earth: a transect back into deep time. In: Geological Survey of Western Australia, Record 2010/21.

Van Kranendonk, M.J., Philippot, P., Lepot, K., Bodorkos, S., Pirajno, F., 2008. Geological setting of Earth's oldest fossils in the ca. 3.5 Ga Dresser Formation, Pilbara Craton, Western Australia. Precambrian Res. 167, 93–124.

Van Kranendonk, M.J., Pirajno, F., 2004. Geochemistry of metabasalts and hydrothermal alteration zones associated with c. 3.45 Ga chert and barite deposits: implications for the geological setting of the Warrawoona Group, Pilbara Craton, Australia. Geochem.: Explor. Environ. Anal. 4, 253–278.

Van Kranendonk, M.J., Smithies, R.H., Hickman, A.H., Champion, D.C., 2007. Paleoarchean development of a continental nucleus: the East Pilbara Terrane of the Pilbara Craton, Western Australia. In: Kranendonk, M.J., Smithies, H.R., Bennett, V.C. (Eds.), Earth's Oldest Rocks. Elsevier, pp. 307–337.

van Zuilen, M.A., Chaussidon, M., Rollion-Bard, C., Marty, B., 2007. Carbonaceous cherts of the Barberton Greenstone Belt, South Africa: isotopic, chemical and structural characteristics of individual microstructures. Geochim. Cosmochim. Acta 71, 655–669.

van Zuilen, M.A., Lepland, A., Teranes, J., Finarelli, J., Wahlen, M., Arrhenius, G., 2003. Graphite and carbonates in the 3.8 Ga old Isua supracrustal belt, southern West Greenland. Precambrian Res. 126, 331–348.

Wacey, D., Kilburn, M.R., Saunders, M., Cliff, J., Brasier, M.D., 2011a. Microfossils of sulphur-metabolizing cells in 3.4-billion-year-old rocks of Western Australia. Nat. Geosci. 4, 698–702.

Wacey, D., Saunders, M., Brasier, M.D., Kilburn, M.R., 2011b. Earliest microbially mediated pyrite oxidation in ~3.4 billion-year-old sediments. Earth Planet. Sci. Lett. 301, 393–402.

Wada, H., Suzuki, K., 1983. Carbon isotopic thermometry calibrated by dolomite-calcite solvus temperatures. Geochim. Cosmochim. Acta 47, 697–706.

Walter, M., Buick, R., Dunlop, J., 1980. Stromatolites 3400–3500 Myr old from the North Pole area, Western Australia. Nature 284, 443–445.

Walter, M., Hofmann, H., Schopf, J., 1983. Geographic and geologic data for processed rock samples. In: Earth's Earliest Biosphere, Its Origin and Evolution., pp. 385–413.

Wopenka, B., Pasteris, J.D., 1993. Structural characterization of kerogens to granulite-facies graphite: applicability of Raman microprobe spectroscopy. Am. Mineral. 78, 533–557.

Williford, K.H., Ushikubo, T., Lepot, K., Kitajima, K., Hallmann, C., Spicuzza, M.J., Kozdon, R., Eigenbrode, L., Summons, R.E., Valley, J.W., 2015. Carbon and sulfur isotopic signatures of ancient life and environment at the microbial scale: Neoarchean shales and carbonates. Geobiology (in press).

Williford, K.H., Ushikubo, T., Schopf, J.W., Lepot, K., Kitajima, K., Valley, J.W., 2013. Preservation and detection of microstructural and taxonomic correlations in the carbon isotopic compositions of individual Precambrian microfossils. Geochim. Cosmochim. Acta 104, 165–182.

Yui, T.F., Huang, E., Xu, J., 1996. Raman spectrum of carbonaceous material: a possible metamorphic grade indicator for low grade metamorphic rocks. J. Metamorph. Geol. 14, 115–124.

Zerkle, A., House, C.H., Brantley, S.L., 2005. Biogeochemical signatures through time as inferred from whole microbial genomes. Am. J. Sci. 305, 467–502.